Volume 8, Issue 15 – e20241018 January – December – 2024

ECORFAN

Journal - Taiwan

ISSN-On line: 2524-2121

15th ANNIVERSARY ECORFAN Special Edition

ECORFAN Journal-Taiwan, Volume 8, Issue 15: e2024815 January - December 2024, is a Continuous publication – ECORFAN-Taiwan, Taipei. YongHe district, Zhong Xin, Street 69. Postcode: 23445. WEB: www.ecorfan.org/taiwan/journal@ecorfan.org. Editor in Chief: Vargas-Delgado, Oscar. PhD. ISSN: 2524-2121. Responsible for the latest update of this number ECORFAN Computer Unit. Escamilla-Bouchán, Imelda. PhD, Luna-Soto, Vladimir. PhD, last updated December 30, 2024.

ECORFAN Journal-Taiwan

Definition of Journal

Scientific Objectives

Support the international scientific community in its written production Science, Technology and Innovation in the Field of Physical Sciences Mathematics and Earth sciences, in Subdisciplines of optical astronomy, optical characterization, optical encoder, experimental research, planetary magnetic fields, ultraviolet radiation, lasers, algorithms and optical waves.

ECORFAN-Mexico, S. C. is a Scientific and Technological Company in contribution to the Human Resource training focused on the continuity in the critical analysis of International Research and is attached to CONACYT-RENIECYT number 1702902, its commitment is to disseminate research and contributions of the International Scientific Community, academic institutions, agencies and entities of the public and private sectors and contribute to the linking of researchers who carry out scientific activities, technological developments and training of specialized human resources with governments, companies and social organizations.

Encourage the interlocution of the International Scientific Community with other Study Centers in Mexico and abroad and promote a wide incorporation of academics, specialists and researchers to the publication in Science Structures of Autonomous Universities - State Public Universities - Federal IES - Polytechnic Universities - Technological Universities - Federal Technological Institutes - Normal Schools - Decentralized Technological Institutes - Intercultural Universities - S & T Councils - CONACYT Research Centers.

Scope, Coverage and Audience

ECORFAN Journal- Taiwan is a Journal edited by ECORFAN-Mexico, S. C. in its Holding with repository in Taiwan, is a scientific publication arbitrated and indexed with semester periods. It supports a wide range of contents that are evaluated by academic peers by the Double-Blind method, around subjects related to the theory and practice of optical astronomy, optical characterization, optical encoder, experimental research, planetary magnetic fields, ultraviolet radiation, lasers, algorithms and optical waves with diverse approaches and perspectives , That contribute to the diffusion of the development of Science Technology and Innovation that allow the arguments related to the decision making and influence in the formulation of international policies in the Field of Physical Sciences Mathematics and Earth sciences. The editorial horizon of ECORFAN-Mexico® extends beyond the academy and integrates other segments of research and analysis outside the scope, as long as they meet the requirements of rigorous argumentative and scientific, as well as addressing issues of general and current interest of the International Scientific Society.

Editorial Board

Arbitration Committee

Assignment of Rights

The sending of an Article to ECORFAN Journal-Taiwan emanates the commitment of the author not to submit it simultaneously to the consideration of other series publications for it must complement the Originality Format for its Article.

The authors sign the Authorization Format for their Article to be disseminated by means that ECORFAN-Mexico, S.C. In its Holding Taiwan considers pertinent for disclosure and diffusion of its Article its Rights of Work.

Declaration of Authorship

Indicate the Name of Author and Coauthors at most in the participation of the Article and indicate in extensive the Institutional Affiliation indicating the Department.

Identify the Name of Author and Coauthors at most with the CVU Scholarship Number-PNPC or SNI-CONACYT- Indicating the Researcher Level and their Google Scholar Profile to verify their Citation Level and H index.

Identify the Name of Author and Coauthors at most in the Science and Technology Profiles widely accepted by the International Scientific Community ORC ID - Researcher ID Thomson - arXiv Author ID - PubMed Author ID - Open ID respectively.

Indicate the contact for correspondence to the Author (Mail and Telephone) and indicate the Researcher who contributes as the first Author of the Article.

Plagiarism Detection

All Articles will be tested by plagiarism software PLAGSCAN if a plagiarism level is detected Positive will not be sent to arbitration and will be rescinded of the reception of the Article notifying the Authors responsible, claiming that academic plagiarism is criminalized in the Penal Code.

Arbitration Process

All Articles will be evaluated by academic peers by the Double Blind method, the Arbitration Approval is a requirement for the Editorial Board to make a final decision that will be final in all cases. MARVID® is a derivative brand of ECORFAN® specialized in providing the expert evaluators all of them with Doctorate degree and distinction of International Researchers in the respective Councils of Science and Technology the counterpart of CONACYT for the chapters of America-Europe-Asia- Africa and Oceania. The identification of the authorship should only appear on a first removable page, in order to ensure that the Arbitration process is anonymous and covers the following stages: Identification of the Journal with its author occupation rate - Identification of Authors and Coauthors - Detection of plagiarism PLAGSCAN - Review of Formats of Authorization and Originality-Allocation to the Editorial Board-Allocation of the pair of Expert Arbitrators-Notification of Arbitration -Declaration of observations to the Author-Verification of Article Modified for Editing-Publication.

Instructions for Scientific, Technological and Innovation Publication

Knowledge Area

The works must be unpublished and refer to topics of optical astronomy, optical characterization, optical encoder, experimental research, planetary magnetic fields, ultraviolet radiation, lasers, algorithms and optical waves and other topics related to Physical Sciences Mathematics and Earth sciences.

Presentation of the content

In the first article we present, *Reconstruction of motor voltage control signal in industrial applications using IoT*, by Camacho-Altamirano, Ulices, Martínez-Carrillo, Irma, Juárez-Toledo, Carlos and Hernández-Epigmenio, Miguel Ángel, with adscription in the Universidad Autónoma del Estado de México - Unidad Académica Profesional Tianguistenco, in the next article we present, *Thermoeconomic analysis in solar collector fields: a focus on constant flowrate and variable flowrate models* by Lugo-Granados, Hebert Gerardo, Canizalez-Dávalos, Lázaro and Picón-Núñez, Martín, with adscription in the Autonomous University of Zacatecas and University of Guanajuato, in the next article we present, *Construction and development of an ultrasonic spray pyrolysis system for semiconductor thin films deposition to photovoltaic applications*, by Palacio-Sifuentes, David, Álvarez-Macias, Carlos, Rodríguez-Castro, Sergio and Martínez-López, Ricardo, with adscription in the Tecnológico Nacional de México/Instituto Tecnológico de La Laguna, in the last article we present, *Effect of the angle of solar irradiance on the photo generation of a photovoltaic module*, by Castillo-Campos, Nohemí Alejandra, Palacio-Sifuentes, David Isaac, Escobedo-Márquez, Diana Laura and Álvarez Macías, Carlos, with adscription in the Tecnológico Nacional de México/Instituto Tecnológico de La Laguna.

Content

Article	Page
Reconstruction of motor voltage control signal in industrial applications using IoT Camacho-Altamirano, Ulices, Martínez-Carrillo, Irma, Juárez-Toledo, Carlos and Hernández-Epigmenio, Miguel Ángel *Universidad Autónoma del Estado de México - Unidad Académica Profesional Tianguistenco*	1-9
Thermoeconomic analysis in solar collector fields: a focus on constant flowrate and variable flowrate models Lugo-Granados, Hebert Gerardo, Canizalez-Dávalos, Lázaro and Picón-Núñez, Martín *Autonomous University of Zacatecas* *University of Guanajuato*	1-12
Construction and development of an ultrasonic spray pyrolysis system for semiconductor thin films deposition to photovoltaic applications Palacio-Sifuentes, David, Álvarez-Macias, Carlos, Rodríguez-Castro, Sergio and Martínez-López, Ricardo *Tecnológico Nacional de México/Instituto Tecnológico de La Laguna*	1-7
Effect of the angle of solar irradiance on the photo generation of a photovoltaic module Castillo-Campos, Nohemí Alejandra, Palacio-Sifuentes, David Isaac, Escobedo-Márquez, Diana Laura and Álvarez Macías, Carlos *Tecnológico Nacional de México/Instituto Tecnológico de La Laguna*	1-7

ECORFAN-Journal Taiwan 8[15]1-9: e1815109
Article

Reconstruction of motor voltage control signal in industrial applications using IoT

Reconstrucción de la señal del control de voltaje de un motor en aplicaciones industriales mediante IoT

Camacho-Altamirano, Ulices* [a], Martínez-Carrillo, Irma [b], Juárez-Toledo, Carlos [c] and Hernández-Epigmenio, Miguel Ángel [d]

[a] Universidad Autónoma del Estado de México - Unidad Académica Profesional Tianguistenco • G-1804-2018 • 0000-0002-4902-6936 • 784595
[b] Universidad Autónoma del Estado de México - Unidad Académica Profesional Tianguistenco • B-9264-2016 • 0000-0002-7952-4418 • 39914
[c] Universidad Autónoma del Estado de México - Unidad Académica Profesional Tianguistenco • C-1368-2016 • 0000-0002-7440-3246 • 39912
[d] Universidad Autónoma del Estado de México - Unidad Académica Profesional Tianguistenco • F-9514-2018 • 0000-0002-1683-4080 • 786771

CONAHCYT classification:

Area: Engineering
Field: Engineering
Discipline: Electronic Engineer
Subdiscipline: Electronics devices

https://doi.org/10.35429/EJT.2024.8.15.1.9
History of the article:
Received: February 02, 2024
Accepted: December 15, 2024

* ✉ [ucamachoa@uaemex.mx]

Abstract

The IIoT allows to have an efficient automation system that monitors specific parts of a system in real time. This paper implements a prototype of speed control and monitoring in a motor belonging to an industrial process with PLC, where the current regulation is related to the data acquisition system and the proposed control algorithm in an IIoT architecture. Finally, the characterization of the starting signal is modeled by means of the angular velocity, the disturbances present in the voltage change and stabilization will be processed using the numerical integration theory and the Matlab tool, to obtain a polynomial approximation of order n.

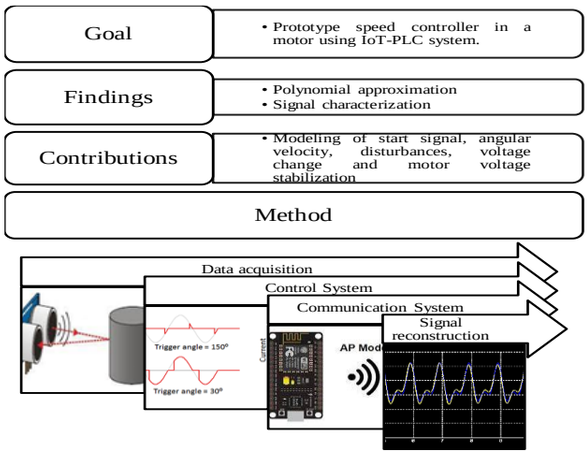

IIoT, Numerical Integration, Polynomial Approximation

Resumen

El IIoT permite tener un sistema de automatización eficaz que monitoree partes específicas de un sistema en tiempo real. Este artículo implementa un prototipo de control y monitorización de velocidad en un motor perteneciente a un proceso industrial con PLC, donde la regulación de corriente está relacionada con el sistema de adquisición de datos y el algoritmo de control propuesto en una arquitectura IIoT. Finalmente se modela la caracterización de la señal de arranque mediante la velocidad angular, las perturbaciones presentes en el cambio de tensión y estabilización serán procesadas usando la teoría de integración numérica y la herramienta de Matlab, para obtener una aproximación polinomial de orden n.

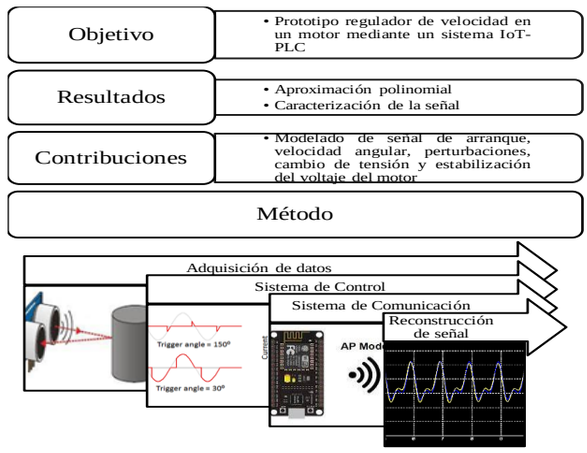

Aproximación polinomial, Integración numérica, IIoT

Citation: Camacho-Altamirano, Ulices, Martínez-Carrillo, Irma, Juárez-Toledo, Carlos and Hernández-Epigmenio, Miguel Ángel. [2024]. Reconstruction of motor voltage control signal in industrial applications using IoT. ECORFAN-Journal Taiwan. 8 [15]1-9: e1815109.

Introduction

The growing trend of the Internet of Things (IoT) is exemplified in new technologies in society, from communication or being able to control home devices remotely, to knowing in real time the location of an online order. According to (Chen et al., 2014) the different applications proposed through the IoT, generate a positive impact for human communication, practically today all the necessary areas are covered in services for businesses and society.

Technological progress through the IoT is reflected in the numerous and diverse applications that have generated an impact since the appearance of the first devices connected to the Internet, today the diversity of applications is the daily life of businesses and society (Hassan et al., 2023).

The recurrent improvement of devices and technology in products and services will have a greater impact on the use of IoT for daily coexistence, (Sarathkumar et al., 2024), mention that Therefore, we use IOT-based techniques to solve issues.

Although the communication paradigm through IoT creates new trends with more technology, where the advancement of applications include, (M2M) Machine to Machine communication, autonomous vehicles, 3D printing, smaller and more efficient sensors, (RFID) radio frequency monitoring, security systems, smart cities, smart grids, smart homes, cyber-medicine, asset management and logistics, agriculture, industrial control and monitoring among others, are some applications that correspond to the rise of IoT (Camacho et al., 2020).

The smart factory is the result of the fusion of the virtual and physical world, where the objective is based on real-time operations, integrated supply chain, virtualization of physical systems for remote monitoring of industrial processes, autonomous and decentralized decision making, prediction of maintenance in equipment connected to the network system, timely response to new demands and changes in the production process according to (El-Gendy,2020).

The importance of IoT applied to industrial processes, especially in Industry 4.0, has allowed companies to be more competitive with the latest advances through the Industrial Internet of Things (IIoT), where industrial processes have been technified worldwide, (Abdullin et al., 2020) defines IIoT as the set of sensors, instruments and autonomous devices connected through the Internet focused on industrial applications, which allows to collect data, perform analysis and optimize production, increase efficiency, reduce costs in the manufacturing process and provide services. For (Milić & Babić, 2020) the IIoT is a fundamental part of Industry 4.0, where the connection between physical and virtual systems allows, to collect data, increase efficiency, optimize production, perform analysis and reduce costs in the manufacturing process and provide services.

Figure 1 shows some applications where IIoT connects machines and devices in industries such as oil, gas, utilities, manufacturing, robotics applications, autonomous vehicles, integration of sensors in machines and tools described by (Jaidka et al., 2020).

Box 1

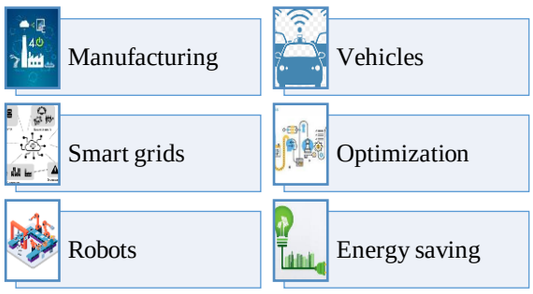

Figure 1

Applications of IIoT systems

Source: (Jaidka et al., 2020)

According to (Tintelecan et al.,2020), electric motors are used to convert electrical energy into mechanical energy, however, they are vulnerable to operating problems generated by long times of use, their commercial, residential and industrial applications require the design of devices to control the improvement in energy consumption (Verma et al.,2024).

The development and improvement systems in more efficient electric motors in the industrial sector driven by strict regulations on electrical energy consumption and reduction of operating costs in production processes set the basis for the improvement of low-cost devices (Awais et al., 2019).

ISSN: 2524-2121.
RENIECYT-CONAHCYT: 1702902

Camacho-Altamirano, Ulices, Martínez-Carrillo, Irma, Juárez-Toledo, Carlos and Hernández-Epigmenio, Miguel Ángel. [2024]. Reconstruction of motor voltage control signal in industrial applications using IoT. ECORFAN-Journal Taiwan. 8 [15]1-9: e1815109.
https://doi.org/10.35429/EJT.2024.8.15.1.9

In (Ramirez et al.,2018), states that the main use of motors in the manufacturing industry corresponds to process control, where some variables controlled in industrial processes are temperature, current, voltage, torque, speed and position.

The objective of this work is to reconstruct the starting signal, voltage change and voltage stabilization of the AC motor coupled to the conveyor belt belonging to the industrial process of a PLC, where the travel speed will be determined by varying the speed of the system through a coupling monitored through the IoT platform.

The methodology to be used is described in Figure 2.

Box 2

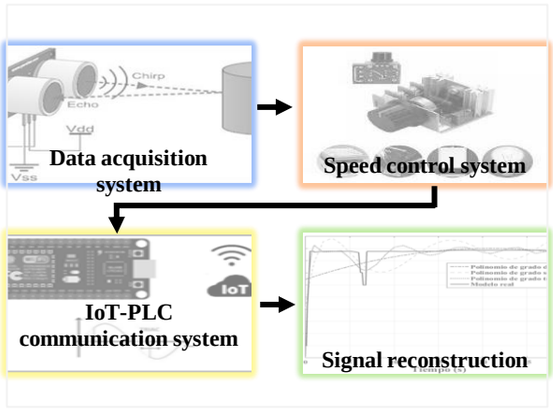

Figure 2

Proposed methodology

Source: Own elaboration

Phase control circuit

(Sharma et al., 2018) refers that regulating devices are used in applications that require control of power, temperature, speed or motor starting, therefore, the control or regulation of power delivered to the load through the thyristor or silicon-controlled rectifier (SCR), is controlled by the trigger potential applied to the gate and the direction of the electric current.

The Triode for Alternating Current or (TRIAC) defined by (Alvarez et al., 2017) is a three-terminal AC semiconductor switch, it is activated in conduction by applying a power signal to the gate electrode, which conducts current in either direction when turned on. The operation of the TRIAC in its conducting state is controlled by the trigger potential applied to the gate and the direction of the electric current is determined by the polarity of the potential it receives according to (Cabrera et al.,2019).

A widely used method for power control is phase control, it consists of a thyristor circuit (DIAC and TRIAC) activated by alternating current, different firing angles generate certain waves of the rectified voltage (Camargo et al., 2017). The voltage wave, the firing and conduction angles are shown in Figure 3, where the electronic switch on high blocks the current flow through controlled intervals, resulting to current supply for the alpha conduction interval (α).

Box 3

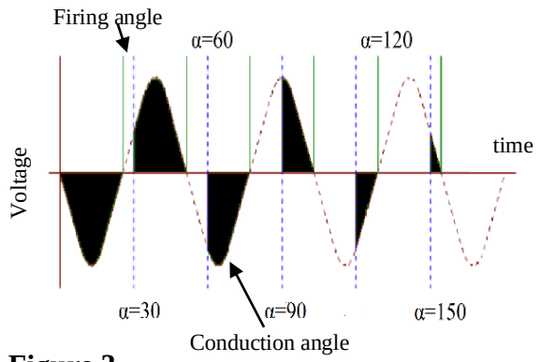

Figure 3

Phase control

Source: (Cabrera et al., 2019)

IIoT system proposed

The combination of architectures, mechanisms and algorithms used in the industrial factory for monitoring and control activities of industrial processes, is established as the pillar of the Industrial Internet of Things (IIoT), to achieve the goal of industrial monitoring and control in motors, machines and devices used in industry facilities (Kolisnyk et al., 2022). The correct operation of the system in industrial processes is based on the continuous monitoring of sensors that collect the relevant data of the process through the Industrial IoT system according to (Duarte dos Santos et al., 2022). As IIoT systems are used more frequently in production processes, the system becomes more secure by monitoring real-time data from the PLC (Ali et al., 2020).

In this work, the procedure to regulate the motor speed is proposed, using the ARDUINO family microcontroller shown in Figure 4. The device conformed by the phase angle control TRIAC circuit is used to feed a single-phase induction motor; where the TRIAC control has a range of variation from a minimum value to the maximum.

ISSN: 2524-2121.
RENIECYT-CONAHCYT: 1702902

Camacho-Altamirano, Ulices, Martínez-Carrillo, Irma, Juárez-Toledo, Carlos and Hernández-Epigmenio, Miguel Ángel. [2024]. Reconstruction of motor voltage control signal in industrial applications using IoT. ECORFAN-Journal Taiwan. 8 [15]1-9: e1815109.
https://doi.org/10.35429/EJT.2024.8.15.1.9

The electrical coupling is the control structure where the obtained data is processed by the algorithm that relates the input and output values, the data obtained by the ESP8266 NodeMCU Wi-Fi card provides the necessary information for speed monitoring.

Box 4

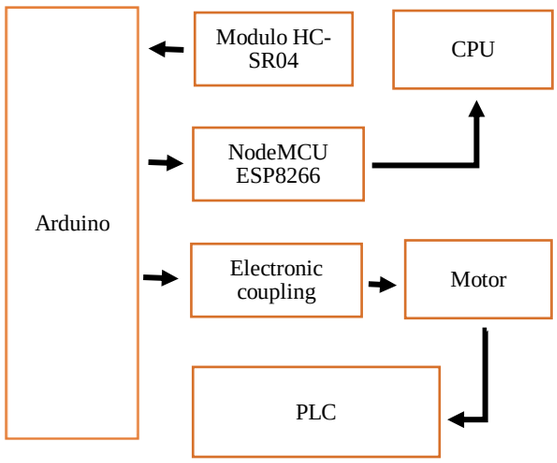

Figure 4
Proposed IIoT system
Source: Own elaboration

Figure 5 (a) corresponds to the elements of the electrical coupling of the IIoT system where, Data acquisition system (1), Speed control system (2) and, IIoT-PLC communication system (3). While Figure 5 (b) shows the elements of the SIMATIC S7-200 PLC proposed for the study where, Pneumatic system for piston actuator (1), Three-phase motor (2), Material feed tower (3), Solenoid valve system (4) and, S7-200 CPU (5).

Box 5

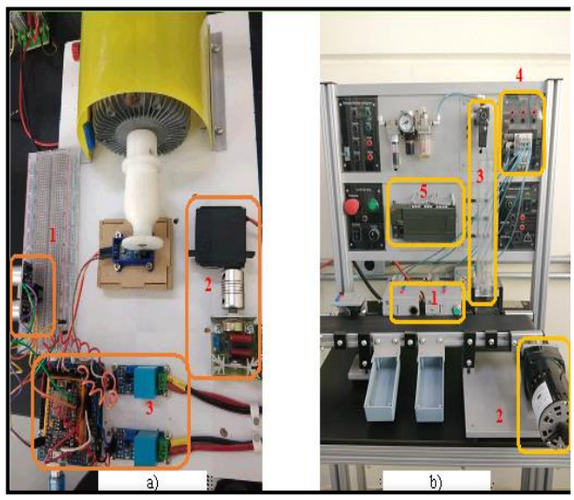

Figure 5
IIoT electronic coupling
Source: Own elaboration

Lab tests

The technique of speed regulation in motors using the voltage-frequency relationship is the proposed control by supplying alternating current through the periodic cut of the sinusoidal signal. The development of the algorithm that establishes the information exchange between the data acquisition system and the proposed control system relates the input and output variables, namely, the distance measured by the ultrasonic sensor is directly proportional to the firing angle.

Figure 5(a) represents the proposed power regulation and motor speed variation system that is activated when the TRIAC controls the passage of alternating current to the load by switching between conduction and firing angles. The conduction angle response for 180°, corresponds to a firing angle α=0°, such that it represents 100% of the motor speed when the material supply of the IIoT system is at maximum capacity.

Figure 6 shows the laboratory tests of the proposed control, where the current supply is modified by periodic cuts in the sinusoidal signal. To obtain an approximate 20% reduction of the initial speed, the firing angle calculated by the algorithm is α =30°, and α =60° if a 50% speed reduction is desired.

The firing angle α =120° represents the minimum voltage at which the motor can operate without affecting its performance, corresponding to the torque-speed characteristic, α >120° would imply total motor shutdown.

Box 6

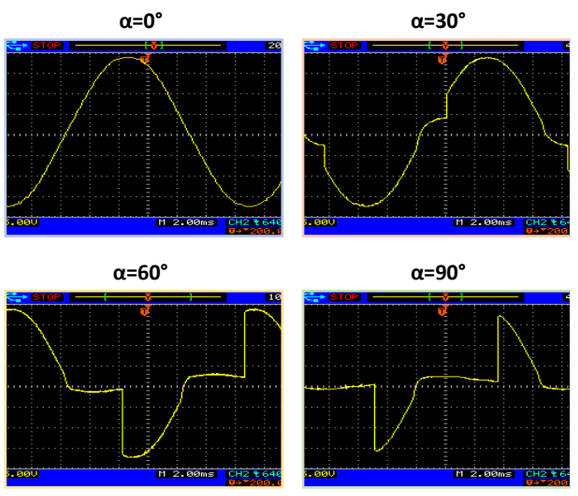

Figure 6
Speed control by firing angle α
Source: Own elaboration

ISSN: 2524-2121.
RENIECYT-CONAHCYT: 1702902

Camacho-Altamirano, Ulices, Martínez-Carrillo, Irma, Juárez-Toledo, Carlos and Hernández-Epigmenio, Miguel Ángel. [2024]. Reconstruction of motor voltage control signal in industrial applications using IoT. ECORFAN-Journal Taiwan. 8 [15]1-9: e1815109.
https://doi.org/10.35429/EJT.2024.8.15.1.9

Polynomial Approximation

Constructing a mathematical function generated by series of data obtained from measurements made by experiments relating two or more variables is the definition of interpolation by (Jorquera & Gelmi, 2014), whose objective is to determine a function that verifies the data and facilitates manipulation due to its simplicity and operability in the area of experimental sciences and engineering.

In (Quezada et al., 2004) the system of equations (1) is used to obtain a polynomial of degree n satisfying the points $y_0, \dots, y_n$, generated by $y_0 = f(x_0),\ y_1 = f(x_1), \dots y_n = f(x_n)$.

$$\begin{cases} a_0 + a_1 x_0 + \cdots + a_n x_0^n = y_0 \\ \vdots \\ a_0 + a_1 x_n + \cdots + a_n x_n^n = y_n \end{cases} \quad [1]$$

Newton's binomial theorem described in (Hernandez et al., 2015) is an arrangement, where equation (2) describes the development of positive powers of a binomial from the k combinations of a group of j elements

$$y_{k+1} = \binom{k}{0} y_{i+1} + \binom{k}{1}\Delta^1 y_1 + \binom{k}{2}\Delta^2 y_1 + \binom{k}{3}\Delta^3 y_1 + \cdots + \binom{k}{k}\Delta^k y_1 \quad [2]$$

as reported in (Cheng-I & Yeong-Chin, 2016) y_k can be expressed as a polynomial of k combinations and degree j.

$$y_{k+1} = a_0 + a_1 k + a_2 k^2 + \cdots + a_j k^j \quad [3]$$

Considering the continuous function at $a \le x \le b$, determine a polynomial $P_n(x_i)$, of degree n shown in equation (4).

$$P_n(x_i) = a_0 + a_1(x) + a_2(x^2) + \cdots + a_n(x^n) \quad [4]$$

Equation (5) expresses the resulting n-order polynomial generated by a system of n defined points

$$y = a_0 + a_1 x + a_2 x^2 + a_3 x^3 + a_4 x^4 + \cdots + a_n x^n \quad [5]$$

where $(a_0, a_1, \dots, a_n)$ correspond to the unknowns required to approximate the polynomial function of equation (5), with this method it is easy to calculate the derivatives and integrals described in (Qui et al., 2016).

Results

The main objective of the polynomial approximation is to find appropriate coefficients to approximate the exact solution. (Zhou et al., 2017) states the idea is to use polynomials up to a certain degree as candidate solutions to find the solution satisfying the given equations at some specific points.

The objective of this work is to obtain a polynomial whose precise, concise and approximate description corresponds to the real behavior of the system generated by the different stages, in order to validate the proposed method where equation (6) takes into account the variability by voltage change.

$$\boldsymbol{x} \in [\boldsymbol{a}, \boldsymbol{b}] \to \mathbb{R}\, \boldsymbol{y}\, \{\boldsymbol{n_0}, \boldsymbol{n_1}, \dots, \boldsymbol{n_m}\} \quad [6]$$

where m is the total number of elements of the angular velocity ω.

Equation (7) corresponds to the number of times that the behavior of the real model described in (Camacho et al., 2023) will be divided.

$$\begin{aligned} \boldsymbol{x_1} &= [\boldsymbol{n_1}, \boldsymbol{n_2}, \dots, \boldsymbol{n_k}] \\ \boldsymbol{x_2} &= [\boldsymbol{n_{k+1}}, \boldsymbol{n_{k+2}}, \dots, \boldsymbol{n_p}] \\ &\vdots \\ \boldsymbol{x_l} &= [\boldsymbol{n_{q+1}}, \boldsymbol{n_{q+2}}, , \dots, \boldsymbol{n_m}] \end{aligned} \quad [7]$$

The relationship between the input and output variables obtained from the laboratory tests corresponds to the firing angle (α) and the angular velocity (ω). Table 1 shows the average measurements of the corresponding to ω over a time interval.

Box 7

Table 1

Parameters of the control and the data system

Firing angle (α) in degrees	Angular velocity (ω) in RPM
0°	3631.79
30°	3024.09
60°	1934.04
90°	492.81

Source: Own elaboration

ISSN: 2524-2121.
RENIECYT-CONAHCYT: 1702902

Camacho-Altamirano, Ulices, Martínez-Carrillo, Irma, Juárez-Toledo, Carlos and Hernández-Epigmenio, Miguel Ángel. [2024]. Reconstruction of motor voltage control signal in industrial applications using IoT. ECORFAN-Journal Taiwan. 8 [15]1-9: e1815109.
https://doi.org/10.35429/EJT.2024.8.15.1.9

Figure 7 shows the signal related between the firing angle and the angular velocity, for the purpose of the study the transformation from revolutions per minute (RPM) to radians per second (rad/s) is performed.

Box 8

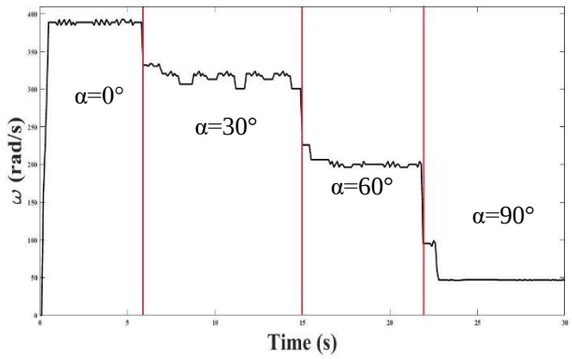

Figure 7

Real model according to firing angle α

Source: Own elaboration

Different stages that the system contemplates during the study period are observed, the first one being the start-up, followed by the voltage changes. The points in Table 2 corresponding to the data collection that satisfy the coefficients of equation (5).

Box 9

Table 2

Coefficients of Equation 5

Coefficient	Result
a_0	-57.22
a_1	1555.34
a_2	-2333.95
a_3	2099.0
a_4	-1279.41
a_5	554.04
a_6	-174.38
a_7	40.63
a_8	-7.13
a_9	0.96
a_{10}	-0.10
a_{11}	0.01
a_{12}	-5.18×10^{-4}
a_{13}	2.59×10^{-5}
a_{14}	-1.01×10^{-6}
a_{15}	3.07×10^{-8}
a_{16}	-7.03×10^{-10}
a_{17}	1.17×10^{-11}
a_{18}	-1.35×10^{-13}
a_{19}	9.65×10^{-16}
a_{20}	-3.18×10^{-18}

Source: Own elaboration

The following shows the resulting polynomial generated in the reconstruction of the angular velocity ω. The polynomial closest to the real behavior of the system is represented in equation (8).

$$f(x) = -57.22 + 1555.34t - 2333.95t^2 + 2099t^3 - 1279.41t^4 + 554.04t^5 - 174.38t^6 + 40.63t^7 - 7.13t^8 + 0.96t^9 - 0.1t^{10} + \cdots - 3.18x10^{-18}t^{20} \quad [8]$$

Figure 8 compares the curve of the real model at different voltage changes with different polynomials, of degrees ten, thirteen and twenty respectively.

Box 10

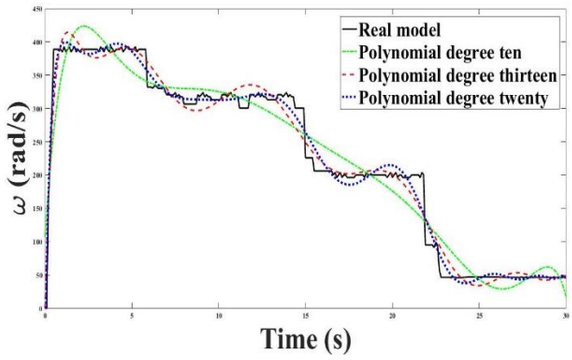

Figure 8

Real model, Polynomial degrees ten, thirteen and twenty

Source: Own elaboration

The polynomial generated by equation (8) represents the curve closest to the real model, the comparison between both is shown in Figure 9.

Box 11

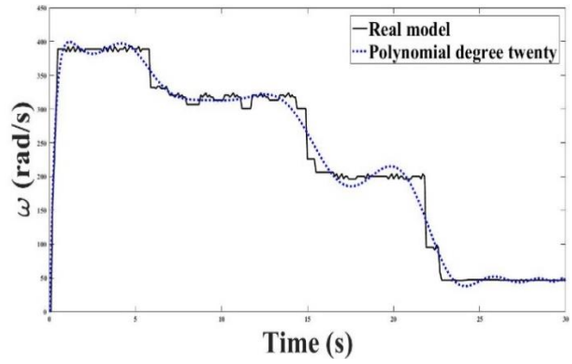

Figure 9

Comparison between the real model and the polynomial model of degree twenty

Source: Own elaboration

ISSN: 2524-2121.
RENIECYT-CONAHCYT: 1702902

Camacho-Altamirano, Ulices, Martínez-Carrillo, Irma, Juárez-Toledo, Carlos and Hernández-Epigmenio, Miguel Ángel. [2024]. Reconstruction of motor voltage control signal in industrial applications using IoT. ECORFAN-Journal Taiwan. 8 [15]1-9: e1815109.
https://doi.org/10.35429/EJT.2024.8.15.1.9

Finally, an additional feature of the proposed method is the possibility to approximate the trajectory in the phase plane, which allows to obtain the stress change behavior of the study model. Equation (9) represents the relation (position θ, velocity ω) belonging to the phase plane.

$$\frac{d\theta/_{dt}}{d\omega/_{dt}} = \frac{\omega(t)}{\alpha(t)} \quad [9]$$

where $\alpha(t)$ is the acceleration in (rad/seg^2) represents a polynomial function of order n corresponding to the numerical approximation obtained from the angular velocity ω.

Figure 10 shows the phase diagram, which clearly indicates the stages of the system behavior.

Box 12

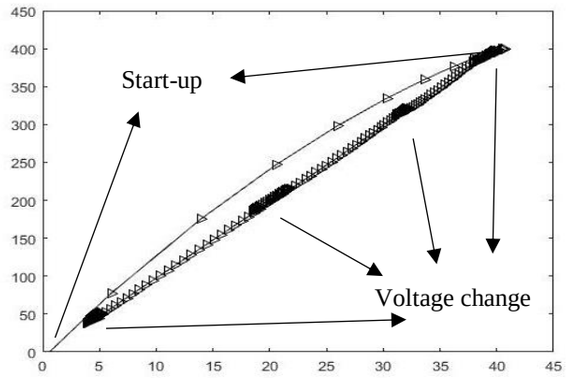

Figure 10
Phase plane of velocity change
Source: Own elaboration

Conclusions

The proposed system uses a single-phase motor, referring to the electrical coupling for control, the implementation allows to work properly with motors of similar characteristics, also meets the objective allowing to control the motor through the configuration provided by the algorithm and the control device interconnected to the IoT network shown in Figure 5.

Polynomials of different degrees are exposed in the work, in order to verify:

- The numerical method based on polynomial equivalents can approximate the physical model represented in Figure 9 where the higher the degree of a polynomial the better approximation to the real model curve is obtained.
- If a better appreciation of the dynamics of the system is desired, it can be represented by sectioning the phenomenon in time windows for each voltage variation and obtain a polynomial approximation of lower degree.

Finally, future work will focus on working on the control of the three-phase motor, this will allow to keep the PLC module without costly and irreversible modifications.

Conflict of interest

The authors declare no interest conflict. They have no known competing financial interests or personal relationships that could have appeared to influence the article reported in this article.

Authors' Contribution

Camacho-Altamirano, Ulices: Contributed to the project idea, method and research technique. Developed the data acquisition system, the speed control algorithm and the writing of the article.

Martínez-Carrillo, Irma: Developed the numerical model for the processing of the data obtained through laboratory tests. Supported the electronic coupling design and the writing of the article.

Juárez-Toledo, Carlos: Contributed in the design of the electronic coupling, the communication protocol of the IIoT system, the method and laboratory tests.

Hernández-Epigmenio, Miguel Ángel: Worked on data acquisition through laboratory tests, numerical model for data processing and debugging of the results.

Availability of data and materials

The electronic coupling and laboratory tests were developed in the automation laboratory of the UAP Tianguistenco of the Universidad Autonoma del Estado de Mexico. The control algorithm and images were obtained from Matlab software.

Funding

The authors are grateful to the Consejo Mexiquense de Ciencia y Tecnología with grant ESYCA2023-144929.

ISSN: 2524-2121.
RENIECYT-CONAHCYT: 1702902

Camacho-Altamirano, Ulices, Martínez-Carrillo, Irma, Juárez-Toledo, Carlos and Hernández-Epigmenio, Miguel Ángel. [2024]. Reconstruction of motor voltage control signal in industrial applications using IoT. ECORFAN-Journal Taiwan. 8 [15]1-9: e1815109.
https://doi.org/10.35429/EJT.2024.8.15.1.9

Abbreviations

3D	Three-Dimensional
AC	Alternating Current
CPU	Central Processing Unit
DIAC	Diode Alternative Current
IIoT	Industrial Internet of Things
IoT	Internet of Things
M2M	Machine to Machine
PLC	Programmable Logic Controller
RFID	Radio Frequency Monitoring
RPM	Revolutions Per Minute
SCR	Silicon-Controlled Rectifier
TRIAC	Triode for Alternating Current
Wi-fi	Wireless Fidelity

References

Basics

Abdullin, V. V., Shnayder, D. A., Khasanov, A. R. and Tselikanov, D. F. (2020). IIoT-Based Approach to Industrial Equipment Condition Monitoring: Wireless Technology and Use Cases. 2020 Global Smart Industry Conference (GloSIC), Chelyabinsk, Russia, 2020, 399-406.

Álvarez, J.D., Araque de los Ríos, O. and Merino, Y. (2017). Electronic device to control the frequency in a single-phase AC motor. Scientia et Techica XXII, 22(4).

Awais, M., Hassan, S. Z., Kamal, T., Zahoor, A., Khan, M. A. and Riaz, M. T. (2019). Control System for Spinning Machine Induction Motor using PLC. 2019 International Conference on Electrical, Communication, and Computer Engineering (ICECCE), Swat, Pakistan, 2019.

Cabrera, J., Juárez, C. y Martínez, I. (2017). Variación del ángulo de disparo de un sistema senoidal para desarrollar un sistema eléctrico de ahorro de potencia. Revista de Investigación y Desarrollo 2017, 3(9), 11-19.

Camacho, U., Martínez, I. and Juárez, C. (2020). Design of an Electronic Coupling to Control Speed of Motor on a Conveyor Belt Using IoT. 2020 International Conference on Mechatronics, Electronics and Automotive Engineering (ICMEAE), Cuernavaca, Mexico, 2020, 115-121.

Camargo, J., Flórez, O. D. and Hernández, J. (2017). A low-cost adjustable speed drive for three phase induction motor. 2017. IEEE Workshop on Power Electronics and Power Quality Applications (PEPQA), Bogota, Colombia, 2017, 1-4.

Chen, S., Xu, H., Liu, D., Hu B. and Wang, H. (2014). A Vision of IoT: Applications, Challenges, and Opportunities with China Perspective. IEEE Internet of Things Journal, 1(4), 349-359. DOI: 10.1109/JIOT.2014.2337336.

Hassan, A. T., Al-Kindi, L. A. H. and Abdulghafour, A. B. (2023). Industrie 4.0 and Smart Manufacturing: A State of the Art Review. 15th International Conference on Developments in eSystems Engineering (DeSE), Baghdad & Anbar, Iraq, 2023, 1-6. DOI: 10.1109/DeSE58274.2023.10100115.

Jaidka, H., Sharma, N. and Singh, R. (2020). Evolution of IoT to IIoT: Applications & Challenges. Proceedings of the International Conference on Innovative Computing & Communications (ICICC) 2020.

Milić, S. D. and Babić, B. M. (2020). Toward the Future—Upgrading Existing Remote Monitoring Concepts to IIoT Concepts. IEEE Internet of Things Journal, 7(12), 11693-11700. DOI: 10.1109/JIOT.2020.2999196.

Ramírez, R., F. Valenzuela, A., Martínez, F., Castañeda, C. E., Morfin, O. A. and Olmos, J. A. (2018). Speed control of a DC motor based on armature current measurement. Ingeniería Investigación y Tecnología, México 2018, 19(4), 1-10.

Sharma, V., Hossain, M. J., Ali, S. M. N. and Kashif, M. (2018). Bi-directional TRIAC fault-protection technique for Z-source half-bridge converter-fed AC motor Drives. 2018 Australasian Universities Power Engineering Conference (AUPEC), Auckland, New Zealand, 2018, 1-6.

Tintelecan, A., Dobra, A. C. and Marțiș, C. (2020). Life Cycle Assessment Comparison of Synchronous Motor and Permanent Magnet Synchronous Motor. 2020 International Conference and Exposition on Electrical And Power Engineering (EPE), Iasi, Romania, 2020, 205-210.

Verma, M., Mitra, A., Bhat, S., Garain, K., Pal, S., & Wankhede, A. K. (2024). An economical and simple strategy for overcoming the Hall sensor faults in three phase brushless DC motor drive. International Journal of Circuit Theory and Applications. DOI: 10.1002/cta.3993.

ISSN: 2524-2121.
RENIECYT-CONAHCYT: 1702902

Camacho-Altamirano, Ulices, Martínez-Carrillo, Irma, Juárez-Toledo, Carlos and Hernández-Epigmenio, Miguel Ángel. [2024]. Reconstruction of motor voltage control signal in industrial applications using IoT. ECORFAN-Journal Taiwan. 8 [15]1-9: e1815109.
https://doi.org/10.35429/EJT.2024.8.15.1.9

Supports

Camacho, U., Martínez, I. and Juárez, C. (2023). Reconstruction of the rotor output signal of a direct current motor using numerical approximation. Journal of Technological Prototypes. 2023. 9(23), 13-22.

Cheng-I., C. and Yeong-Chin, C. (2016). Signal Reconstruction Based on Newton's Forward Divided Difference for SCADA of Wide-Area Intelligent Energy System. 2016 International Symposium on Computer, Consumer and Control, 682-685.

Hernández, I., Juárez, C. y Martínez, I., (2015). Interpolación polinomial para determinar el tiempo de tratamiento criogénico para acero AISI D2 en medio básico. Pistas educativas, 36(112), 1087-1100.

Jorquera, H. and Gelmi, C. (2014). Métodos numéricos aplicados a la ingeniería, casos de estudio en ingeniería de procesos usando MATLAB. Primera edición, Ediciones Universidad Católica de Chile, ISBN: 978-956-14-1482-2, pp. 55.

Quesada, J. M., Sánchez, C., Jódar J., Martínez, J. (2004) Análisis y Métodos Numéricos. 1ra edición. Publicaciones de la Universidad de Jaén, Jaén, ISBN 978-8484392224.

Qui, Y., Wu, H., Zhou, Y., Song, Y. (2016). Global Parametric Polynomial Approximation of Static Voltage Stability Region Bondaries. IEEE Transactions on Power Systems. 32(3), 23

Zhou, Y., Wu, H., Gu, C. and Song, Y., (2017). A Novel Method of Polynomial Approximation for Parametric Problems in Power Systems. IEEE Transactions on power systems, 32(4), 3298-3307.

Differences

Ali, M. A., Miry, A. H. and Salman, T. M. (2020). IoT Based Water Tank Level Control System Using PLC. 2020 International Conference on Computer Science and Software Engineering (CSASE), Duhok, Iraq, 2020, 7-12.

Duarte dos Santos, A., Moreira, R., Vedoveto, A., Dante, A. and Chagas, E. (2022). Simple and Low-Cost PLC Modem for IoT Applications. IEEE Latin America Transactions, 20(12), 2455-2462.

El-Gendy, S. (2020). IoT Based AI and its Implementations in Industries. 2020 15th International Conference on Computer Engineering and Systems (ICCES), Cairo, Egypt, 2020, 1-6.

Kolisnyk, M., Jantsch A. and Piskachova, I. (2022). Markov Model for Availability Assessment of PLC in Industrial IoT Considering Subsystems Failures. 2022 12th International Conference on Dependable Systems, Services and Technologies (DESSERT), Athens, Greece, 2022, 1-4. DOI: 10.1109/DESSERT58054.2022.10018637.

Sarathkumar, D., Raj, R. A., Akbar, S. S., Kanna, R. R., Andrews, L. J. B., & Alagappan, A. (2024). IOT Based Motor Control and Line Detection for Smart Agriculture. In 2024 IEEE International Students' Conference on Electrical, Electronics and Computer Science (SCEECS). 1-6.

ISSN: 2524-2121.
RENIECYT-CONAHCYT: 1702902

Camacho-Altamirano, Ulices, Martínez-Carrillo, Irma, Juárez-Toledo, Carlos and Hernández-Epigmenio, Miguel Ángel. [2024]. Reconstruction of motor voltage control signal in industrial applications using IoT. ECORFAN-Journal Taiwan. 8 [15]1-9: e1815109.
https://doi.org/10.35429/EJT.2024.8.15.1.9

ECORFAN-Journal Taiwan 8[15]1-12: e2815112
Article

Thermoeconomic analysis in solar collector fields: a focus on constant flowrate and variable flowrate models

Análisis termoeconómico en campos de colectores solares: un enfoque en los modelos de flujo constante y flujo variable

Lugo-Granados, Hebert Gerardo*[a], Canizalez-Dávalos, Lázaro[b] and Picón-Núñez, Martín[c]

[a] Autonomous University of Zacatecas • F-2050-2019 • 0000-0002-0027-3418 • 487049
[b] Autonomous University of Zacatecas • ABW-3215-2022 • 0000-0002-3126-8574 • 164509
[c] University of Guanajuato • AHA-5481-2022 • 0000-0002-0793-192X • 12408

CONAHCYT classification:

Area: Engineering
Field: Engineering
Discipline: Mechanical Engineering
Subdiscipline: Energy

https://doi.org/10.35429/EJT.2024.8.15.1.12
History of the article:
Received: February 25, 2024
Accepted: December 19, 2024

* ✉ [lugh871024@gmail.com]

Abstract

In this study, the operation models with constant flowrate and variable flowrate of a flat-plate solar collector field are analysed. The model that achieves greater energy utilization and lower operating costs was determined under two conditions: when scaling fouling occurs in the collector tubes and when a clean operation (without fouling) is considered. The case study involves a pasteurization plant operating at temperatures above 85°C. The operational scenarios are as follows: 1) Variable flowrate: the flowrate is adjusted based on environmental conditions to maintain a constant outlet temperature, and 2) Constant flowrate: the flowrate remains constant, resulting in varying collector outlet temperatures depending on weather conditions. The results show that under clean conditions, operating with variable flowrate yields a lower cost per kWh of captured energy ($0.048/kWh). In the presence of fouling, the cost of operating with variable flowrate significantly increases to $0.15/kWh, while constant flowrate results in the lowest cost ($0.077/kWh).

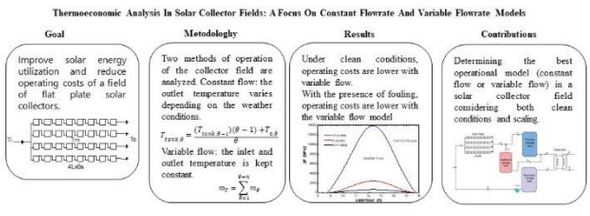

Collectors, Networks, Scaling

Resumen

En el presente trabajo se analizan los modelos de operación con flujo constante y flujo variable de un campo de colectores solares de placa plana. Se determinó el modelo que presenta mayor aprovechamiento de energía y menores costos de operación en dos condiciones, cuando se tiene ensuciamiento por scaling en los tubos del colector y cuando se considera una operación limpia (sin ensuciamiento). El caso de estudio es una planta pasteurizadora que opera a temperaturas mayores a 85°C. Los escenarios de operación son: 1) Flujo variable: el flujo se modifica en función de las condiciones ambientales para mantener la temperatura de salida constante y 2) Flujo constante: se mantiene constante el flujo, por lo que la temperatura a la salida de los colectores varía en función de las condiciones climatológicas. Los resultados muestran que en condiciones limpias al operar con flujo variable se obtiene un menor costo por kWh de energía capturada (0.048$/kWh). En presencia de ensuciamiento el costo de operar con flujo variable aumenta considerablemente a 0.15$/kWh, mientras que con flujo variable se obtiene el menor costo (0.077 $/kWh).

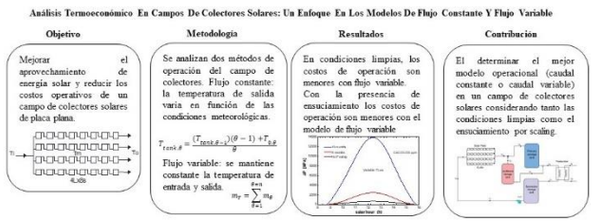

Colectores, Redes, Scaling.

Citation: Lugo-Granados, Hebert Gerardo, Canizalez-Dávalos, Lázaro and Picón-Núñez, Martín. [2024]. Thermoeconomic analysis in solar collector fields: a focus on constant flowrate and variable flowrate models. ECORFAN-Journal Taiwan. 8 [15]1-12: e2815112.

Introduction

In this work, we aim to understand the operating model (constant flowrate or variable flowrate) of a solar collector field that achieves optimal thermal performance and lower operating costs.

Operating with a constant flowrate model allows leads to higher temperatures than required by the process, resulting in excess thermal load. On the other hand, operating with variable flowrate leads to attain more hot water than necessary, also leading to excess thermal load. Increasing the water flowrate through the collectors results in additional pressure drops and consequently raises operating costs.

The excess thermal load obtained can be stored for use when there is a solar energy deficit or to increase production.

When designing a solar collector network, it is necessary to consider the climatic variations that occur during a typical solar day, such as air velocity, solar radiation, ambient temperature, etc. However, the design should always prioritize energy utilization and minimize energy losses. In the case of the pasteurization process, it is challenging to avoid energy losses because the collector inlet temperatures must exceed 75°C (Hanson et al., 2005). This condition requires high solar radiation (<550W/m²) to produce thermal energy at these temperatures.

Weather conditions, for example: poor solar radiation, low ambient temperatures, and high air velocities, as well as scaling fouling, are parameters that directly affect the thermal and hydraulic performance of solar collectors (Bunea et al., 2012). Over time, scaling fouling also causes thermal and hydraulic problems by depositing mineral salts (CaCO3) inside the tubes.

Operating variables (volumetric flowrate rate, inlet temperature, and operating time) are parameters that can be modified to improve the performance of solar collectors. When the radiation level is lower than that used for network design, the outlet temperature of the collectors is lower than the inlet temperature, resulting in thermal energy loss. To prevent energy losses when radiation decreases, the flowrate velocity can be adjusted based on weather conditions.

Various authors have reported works where they have analysed the influence of operating variables and climatic conditions on the thermal performance of solar collectors. Dembeck-Kerekes et al. (2019) introduced a strategy for variable flowrate control in a thermal-photovoltaic collector to optimise energy generation. Sokhansefat et al.

(2018) found that inlet temperature and climatic conditions are the main variables affecting the performance of a solar collector when operating in cold weather. Climatic conditions significantly impact solar energy utilization. Zhuang et al. (2024) determined that radiation has a greater impact compared to other parameters. However, all climatic conditions must be considered to ensure robust designs, analyses, and results.

There are studies focused on developing models to determine the performance of a flat plate solar collector considering the effects of solar radiation, mass flow rate, and the geometric parameters. Majumdar et al. (2020) conducted research in this area. Unterberger et al. (2021) and Momodu-Bangura et al. (2022) determined the performance of a flat plate collector and a double-pass solar collector through the cover, respectively, by varying solar radiation and ambient temperature. Du et al. (2022) presented a method that combines input data such as solar radiation, ambient temperature, air velocity, fluid flow rate, and fluid inlet temperature with an artificial neural network model to improve the accuracy of vacuum tube solar collectors' performance. Wang et al. (2021) proposed a numerical model to analyse the effects of network configuration, flowrate, inlet temperature, and working fluid on pressure drops and outlet temperatures in a field of flat plate solar collectors.

Studies reported so far, do not consider scaling fouling in their models or experimental results. In the literature, there are few studies that include scaling fouling in the operation of solar collectors. Arunachala et al. (2015) provided an overview of the effects caused by radiation and scaling fouling on the instantaneous efficiency variation of a solar collector. Lugo-Granados et al. (2023) investigated the effects of scaling fouling on the thermohydraulic performance of a network of solar collectors.

ISSN: 2524-2121.
RENIECYT-CONAHCYT: 1702902

Lugo-Granados, Hebert Gerardo, Canizalez-Dávalos, Lázaro and Picón-Núñez, Martín. [2024]. Thermoeconomic analysis in solar collector fields: a focus on constant flowrate and variable flowrate models. ECORFAN-Journal Taiwan. 8 [15]1-12: e2815112.
https://doi.org/10.35429/EJT.2024.8.15.1.12

In 2024, Lugo-Granados et al. determined the optimal network design for a field of solar collectors in terms of operational costs and thermal load acquisition, both under clean conditions and when scaling fouling is present.

These studies maintain constant operating parameters such as volumetric flow rate and climatic conditions (ambient temperature and air velocity). Variations in these parameters can mitigate the effects caused by scaling fouling and enhance the performance of the solar collector network.

The contribution of this research consists of determining the best operational model within two scenarios: constant flowrate and variable flowrate in a field of flat plate solar collectors to provide thermal load to a pasteurization plant. Additionally, the goal is to identify the model that enhances solar energy utilization and results in the lowest operating costs, considering both clean conditions and scaling fouling.

Case study: Pasteurization plant

The case study involves a thermosolar plant responsible for supplying thermal load to a milk pasteurization process (2010). A total of 3,500 liters of milk are pasteurized daily. The entire amount of water heated during the day is used to perform pasteurization at 7:00 a.m. the following day.

Figure 1 shows the operational diagram of the pasteurization plant. The installation consists of a primary circuit composed of the solar collector field and storage tanks, which connect to the secondary thermal treatment circuit. The secondary circuit has three stages: pasteurization, recovery, and cooling. Hot water obtained from the solar collector field is stored in the primary container at 82°C. It then passes through the pasteurizer exchanger, where its temperature drops to 76°C. Finally, it is stored in the secondary container to circulate back through the collectors.

Meanwhile, the milk enters the pasteurizer at a temperature of 72°C and exits at 80°C. The hot water leaving the solar collectors must have a temperature higher than 82°C to ensure pasteurization.

During the pasteurization process, the milk temperature must be raised to 72-75°C and maintained at the same temperature for 15 to 20 seconds. In the recovery and heat-saving stage, cold (unpasteurized) milk is preheated with the hot outlet milk (pasteurized).

In the cooling stage, the milk temperature is reduced below 4°C.

Box 1

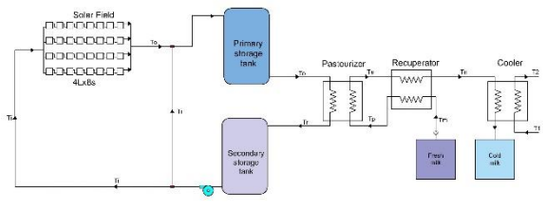

Figure 1
Pasteurization plant diagram

The solar field consists of 32 collectors divided into 4 rows, each with 8 collectors connected in series (4Lx8s), where the letters 'L,' 'p,' and 's' indicate line, parallel, and series, respectively (Figure 2). The number of collectors in series ensures that around 30% of the solar hours in a year, the water temperature at the outlet of the last collector in series will be above 80°C.

The working period for the solar collectors is 8 hours, from 8:00 in the morning until 16:00 in the afternoon. The total water flowrate passing through the collector network is 401.12 liters per hour, resulting in a daily storage of 3,209 liters of hot water. The water flowrate required to pasteurize 3,500 liters of milk within an hour must be equal to or greater than this amount for effective heat exchange.

In the Table 1 shows main features of flat plate solar collectors.

Box 2

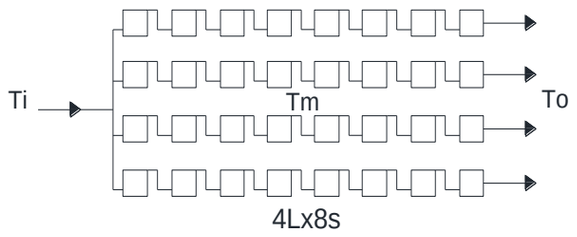

Figure 2
Configuration of the solar collector network

ISSN: 2524-2121.
RENIECYT-CONAHCYT: 1702902

Lugo-Granados, Hebert Gerardo, Canizalez-Dávalos, Lázaro and Picón-Núñez, Martín. [2024]. Thermoeconomic analysis in solar collector fields: a focus on constant flowrate and variable flowrate models. ECORFAN-Journal Taiwan. 8 [15]1-12: e2815112.
https://doi.org/10.35429/EJT.2024.8.15.1.12

Box3

Table 1

Main geometrical features of flat plate solar collectors

Dimensions	**Length**	**width**	**Absorber / Total area**
	2,190 (mm)	1,090 (mm)	2.13 (m^2) / 2.40 (m^2)
Absorber tube	**Number of tubes**	**External diameter**	**Internal diameter**
	10	10 (mm)	8 (mm)
Cover	**Material**	**Transmittance**	**Thickness**
	Tempered solar glass	0.91	3.20 (mm)
Absorber	**surface absorptivity**	**Thickness**	**Surface Emissivity**
	0.95	0.4 (mm)	0.05
Tubes collectors	**Number of tubes**	**External diameter**	**Internal diameter**
	2	22 (mm)	20 (mm)
Insulating and shell	**Bottom insulation thickness**	**Side insulation thickness**	**Material**
	30 (mm)	30 (mm)	Polyurethane + mineral wool

Methodology

Operation modes: Constant flowrate and variable flowrate

The operation of the solar collector field is a continuous process. The secondary tank feeds the solar field during the day at a constant inlet temperature, Ti (°C). The useful heat quantity, Qu (kW), obtained from the collectors can be determined from Eqs. 1 to 7.

$$Q_{u,\theta} = \dot{m}_{f,\theta}\, C_{p,\theta}(T_{0,\theta} - T_{i,\theta}) \quad (1)$$

$$Q_{u,\theta} = F_{R,\theta} A_{s,\theta}\left[I_{G,\theta}(\tau\alpha_c) - U_{c,\theta}\left(T_{pm,\theta} - T_{a,\theta}\right)\right] \quad (2)$$

Where Θ is the cycle iteration, As (m^2) is the plate surface area, $\dot{m}_f$ (kg/s) is the mass flowrate, C_p (kJ/Kg°C) is the specific heat, T_i and T_0 (°C) are the inlet and outlet temperature in the tubes respectively. (F_R) is the heat removal factor from the plate to the fluid, T_{pm} (°C) is the temperature of the plate and T_a (°C) is the ambient temperature (°C), (α_c y τ) are the absorbance and transmittance of the transparent cover and the term I_G (W/m^2) is the solar radiation intensity.

In Eq. (3), the heat removal factor FR is presented, which depends on the overall heat transfer coefficient Uc (W/m²°C) and the collector efficiency factor F' (Eq. 4).

$$(4))\ F_{R,\theta} = \frac{\dot{m_{f,\theta}} C_{P,\theta}}{A_S\, U_{c,\theta}}\left[1 - e^{\frac{-A_S\, U_{c,\theta} F_\theta^{'}}{\dot{m}_f C_{P,\theta}}}\right] \quad (3)$$

The collector efficiency factor primarily depends on the resistance to heat transfer from the absorber plate to the working fluid. These resistances manifest through the junction between the plate and the tube, denoted as C_b (m² °C/W) in Eq. (5). They arise due to the tube wall (Rt, m² °C/W), fouling layer (Rs, m² °C/W), and the convection resistance between the tube's inner wall and the working fluid (Rh, m² °C/W). Additionally, it is influenced by the fin efficiency (FA), expressed in Eq. (6).

$$F_\theta^{'} = \frac{1/U_{c,\theta}}{S\left[\frac{1}{U_{c,\theta}\left[d_0 + F_{A,\theta}(S-d_0)\right]} + \frac{1}{C_{b,\theta}} + \frac{R_{h,\theta}}{\pi d_{s,\theta}} + \frac{R_{t,\theta}}{\pi d_{s,\theta}} + \frac{R_{s,\theta}}{\pi d_{s,\theta}}\right]} \quad (4)$$

$$C_{b,\theta} = \frac{k_{b,\theta} W}{\gamma} \quad (5)$$

Where k_b represents thermal conductivity, W (m) is the width of the junction, and γ (m) is the thickness of the junction between the plate and the tube. d_i and d_0 (m) denote the inner and outer diameters, S (m) is the distance between tubes.

$$F_{A,\theta} = \frac{Tanh[M(S-d_0)/2]}{M_\theta(S-d_0)/2} \quad (6)$$

While M (m^{-1}) is expressed in Eq.(7), where K_s (W/m°C) and δ (m) are the thermal conductivity and the plate thickness.

$$M_\theta = \sqrt{\frac{U_{c,\theta}}{K_s \delta}} \quad (7)$$

The instantaneous efficiency (η) of the collectors is determined from Eq.(8).

$$\eta_\theta = \frac{Q_{u,\theta}}{I_{G,\theta} A_s} \quad (8)$$

The total heat load Q_T (kW) stored in the tank is the sum of the thermal load per cycle, Eq.(9).

$$Q_T = Qu,1 + Qu,2 + Qu,3 + \cdots + Qu,n \quad (9)$$

ISSN: 2524-2121.
RENIECYT-CONAHCYT: 1702902

Lugo-Granados, Hebert Gerardo, Canizalez-Dávalos, Lázaro and Picón-Núñez, Martín. [2024]. Thermoeconomic analysis in solar collector fields: a focus on constant flowrate and variable flowrate models. ECORFAN-Journal Taiwan. 8 [15]1-12: e2815112.
https://doi.org/10.35429/EJT.2024.8.15.1.12

A mathematical model developed by Lugo-Granados et al. (2018) was implemented to determine the amount of scaling (CaCO3) deposited in the tubes of solar collectors. Eq. 10 describes this process.

$$\dot{m}_{d,\theta} = \frac{\beta}{2}\left(\frac{\beta,\theta}{\alpha\, k_{r,\theta}} + (C_1 + C_2) - \sqrt{\frac{[\beta,\theta+(C_{1+}C_2)\,\alpha,\theta\, k_{r,\theta}]^2+4\,\alpha_\theta^2\, k_{r,\theta}{}^2(K_{sp,\theta}-[C_1][C_2])}{\alpha_\theta^2\, k_{r,\theta}{}^2}}\right) \quad (10)$$

The model calculates the mass flux $\dot{m}_d$ (kg/m^2 s) of $CaCO_3$ deposited inside the tubes, considering parameters involved in scaling formation such as pH, the concentration of Ca_2+ (C1) (kg/m^3), CO_3^{2-} (C2) (kg/m^3), and the solubility Ksp (kg^2/m^6) of CaO_3 in water.

The model also incorporates the chemical reaction constant k_r (m^2/kg s), which describes the rate of crystal formation. Another variable is the mass transfer coefficient β (m/s). Additionally, the dimensionless deposition resistance factor α (Eq. 10) accounts for viscous and inertial effects affecting crystal deposition on the surface. Over time, fouling increases, leading to changes in tube roughness and diameter, resulting in greater pressure drop.

$$\alpha_\theta = \frac{191}{f \cdot Re^{1.67}} \quad (10)$$

The calculation of the mass flux, $\dot{m}_d$ (kg/m² s), deposited allows determining the thermal resistance generated by fouling during the operation of solar collectors using Eq. (11). According to this expression, the thermal resistance due to fouling, Rs (m² °C/W), is also a function of the mass flux that is removed, $\dot{m}_r$ (kg/m² s), Quan, et al. (2008); the density ρ_f (kg/m³) and the thermal conductivity λ_f (W/m °C) of $CaCO_3$.

$$\frac{dR_{s,\theta}}{dt,\theta} = \frac{\dot{m}_d - \dot{m}_r}{\rho_f \lambda_f} \quad (11)$$

When operating with the constant flowrate model, the outlet temperature varies in each cycle based on climatic conditions and the presence of scaling fouling. Therefore, the obtained useful load Q_u (kW) depends solely on the outlet temperature, T_0 (°C).

The temperature reached by the water in the storage tank ($T_{tank,\Theta}$) results from the mixture of water leaving the collectors in each cycle ($T_{0,\Theta}$) and the tank temperature obtained in the previous cycle ($T_{tank,\Theta-1}$), Eq. (12).

$$T_{tank,\theta} = \frac{(T_{tank,\theta-1})(\theta-1)+T_{0,\theta}}{\theta} \quad (12)$$

For the variable flowrate model, the amount of water $\dot{m}_f$ (kg) passing through the solar collector field varies based on environmental conditions and scaling fouling to maintain a constant outlet temperature T_o (in °C).

Therefore, the useful heat (Q_u (kW)) obtained from the collectors depends solely on the water flowrate, as described by Equation 1. The mass deposited in the storage tank during each cycle *m* (kg) depends on the mass flow rate $\dot{m}_f$ (kg/s) in each cycle and the cycle time, t (s) as given by Eq.13.

$$m_{,\theta} = \dot{m}_{f,\theta} \cdot t_\theta \quad (13)$$

The total mass m_T (kg) is the summation of each cycle, Eq. (14). The mass excess is storage in an additional tank (Figure 3).

$$m_T = \sum_{\theta=1}^{\theta=n} m_\theta \quad (14)$$

For the variable flowrate model, pressure drop varies in each cycle. Starting from Eq. (15), we obtain the pressure drop within the collector network, which is proportional to the sum of hydraulic resistances K_i (kPa s²/m⁶) and the square of the volumetric flow rate $\dot{V}$ (m³/s).

$$\Delta P_{T,\theta} = \dot{V}_\theta^2 \sum_{i=1}^{n} K_i \quad (15)$$

Eqs. (16 and 17) show the main hydraulic resistances. The resistance generated by friction, denoted as K_1 (kPa s²/m⁶), is due to the pipe length. Additionally, the resistance generated by accessories, represented by K_2 (kPa s²/m⁶), such as elbows, valves, and unions, is considered.

$$K_{1,\theta} = \frac{8L_t}{\pi^2(d_{s,\theta})^5} f_\theta \quad (16)$$

$$K_{2,\theta} = \frac{8\rho}{\pi^2(d_{s,\theta})^5} k_f \quad (17)$$

ISSN: 2524-2121.
RENIECYT-CONAHCYT: 1702902

Lugo-Granados, Hebert Gerardo, Canizalez-Dávalos, Lázaro and Picón-Núñez, Martín. [2024]. Thermoeconomic analysis in solar collector fields: a focus on constant flowrate and variable flowrate models. ECORFAN-Journal Taiwan. 8 [15]1-12: e2815112.
https://doi.org/10.35429/EJT.2024.8.15.1.12

where f is the friction factor along the pipe, k_f, is the resistance factor for each accessory, L_t (m) and d_s (m) are the length and hydraulic diameter of the tube. It is observed that reducing the diameter increases flow resistance, leading to higher pressure drop.

Box 4

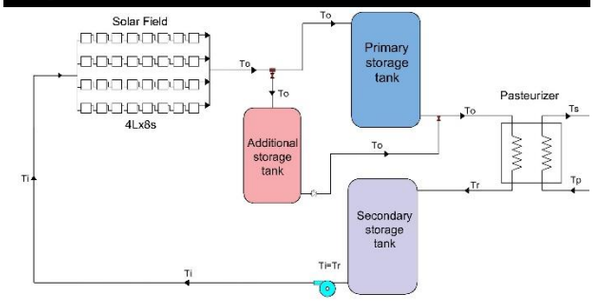

Figure 3

Primary circuit of the pasteurizer plant with energy storage

Cost Model

The total operating cost $Cost_{total}$ ($) is the sum of pumping costs per cycle and the annualized cost of collectors, Eq. (18).

$$Cost_{total} = Cost_b + Cost_a \quad (18)$$

The pump operating cost $Cost_b$ ($) is directly proportional to pump power, operation time t (h), and the unit cost of electricity Costu ($/kWh). Eq. (19) assumes an electricity cost of $0.3/kWh.

$$Cost_{b,\theta} = cost_u \dot{w}_\theta \, t \quad (19)$$

Pump power depends on volumetric flow rate $\dot{V}$ (m^3/s), pump pressure drop ΔP (kPa), and pump efficiency (ηb), Eq.(20).

$$\dot{w}_\theta = \frac{\dot{V}_\theta \Delta P_\theta}{\eta_b} \quad (20)$$

The Annualised Cost of Collectors ($Cost_a$) is equal to the cost per collector Cu ($) multiplied by the annualization factor Ƒa and the total number of collectors ((Nc)), Eq.(21). The estimated commercial cost per collector is $811.76 USD. To calculate the annualization factor ((Ƒa)), we consider a collector lifespan (ω) of 20 years and an annual interest rate ï of 8%. Eq.(22).

$$Cost_a = C_u \cdot Fac_A \cdot N_c \quad (21)$$

$$Ƒ_a = \left[\frac{ï(1+ï)^\omega}{(1+ï)^\omega - 1}\right] \quad (22)$$

Results

Climate Conditions

Graph 1 depicts ambient temperature and air velocity throughout a typical spring day in central Mexico. The minimum ambient temperature is 17°C, and the maximum is 32°C. Air velocity varies from 2.2 m/s to 10 m/s.

Graph 2 illustrates solar radiation over the course of the day, reaching a peak value of 1,106 W/m² at 12:45 h.

Box 5

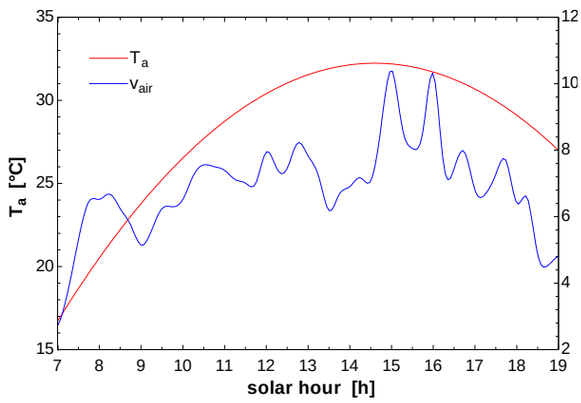

Graph 1

Typical variation of ambient temperature and wind velocity with solar time (Central Mexico)

Box 6

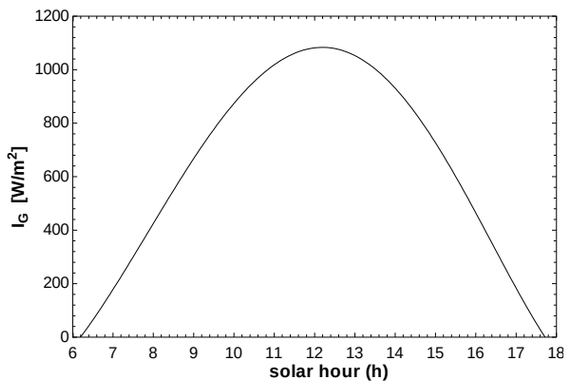

Graph 2

Solar radiation with respect to solar time.

Graph 3 presents graphs of the outlet temperature from a collector field relative to ambient temperature for different air velocities.

ISSN: 2524-2121.
RENIECYT-CONAHCYT: 1702902

Lugo-Granados, Hebert Gerardo, Canizalez-Dávalos, Lázaro and Picón-Núñez, Martín. [2024]. Thermoeconomic analysis in solar collector fields: a focus on constant flowrate and variable flowrate models. ECORFAN-Journal Taiwan. 8 [15]1-12: e2815112.
https://doi.org/10.35429/EJT.2024.8.15.1.12

The inlet temperature, volumetric flow rate, and solar radiation remain constant. Under these conditions, a 10°C increase in ambient temperature leads to a 1°C rise in outlet temperature across various air velocities. Additionally, increasing air velocity from 6 m/s to 10 m/s reduces the outlet temperature by 0.3°C.

Graph 4 shows that a 1 m/s increase in air velocity the solar collector's outlet temperature decreases by 0.1°C.

Box 7

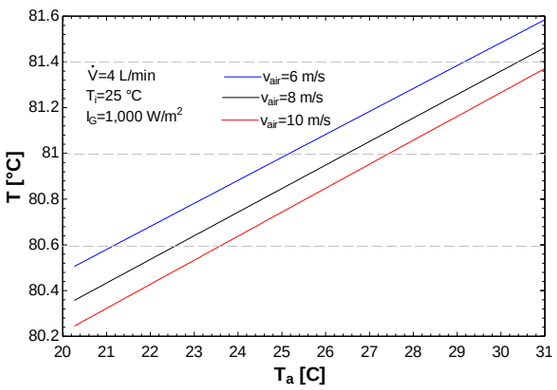

Graph 3

Fluid outlet temperature for different fluid mass flow rate

Box 8

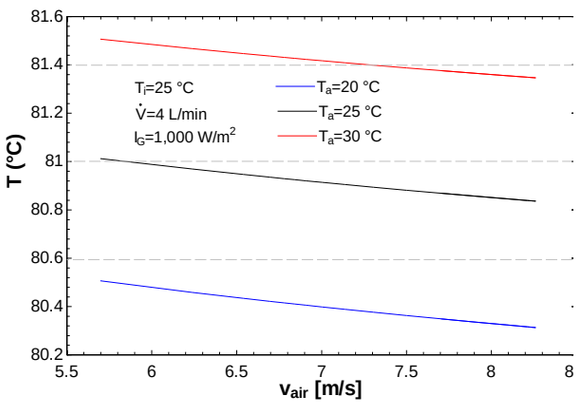

Graph 4

Fluid outlet temperatura with respect to air velocity for differnt ambient temperature

Network design

An analysis was conducted to determine the appropriate network design for raising the temperature from 75°C to 85°C with a total volumetric flow rate of 6.685 L/min. The network design involves determining the number of collectors per line connected in series to achieve the target temperature. The network should consist of 4 lines to provide the necessary thermal load.

From the obtained results (Graph 5), it is found that to reach the target temperature (85°C), operation is required with radiation greater than 550 W/m², as under these conditions, the maximum temperature reached is 84.5°C with 51 collectors in series per line. When there is a radiation of 575 W/m², 17 collectors per line are needed to reach the target temperature. Increasing radiation reduces the required number of collectors to achieve the target temperature.

With radiation of 625 W/m², 8 collectors are needed to achieve a temperature of 85°C, representing a 53% reduction in area compared to designing with radiation of 575 W/m² (17 collectors). Consequently, the start time for operating the collector network should be delayed by approximately 15 minutes to obtain a radiation of 625 W/m² (see Figure 5).

On the other hand, having a solar field with 17 collectors per line results in greater energy gain but also higher costs. According to Lugo-Granados et al. [XI], Rs-p represents the ratio between the number of lines (N_L) and parallel collectors (Np) to the quantity of series collectors (N_p). A value of R_{s-p} closer to 1 indicates better performance of the network from a thermohydraulic and economic perspective. When there are 8 collectors per line, the R_{s-p} value is 2, whereas with 17 collectors per line, R_{s-p} = 4.25. Based on this, the network design with 8 collectors is superior.

$$R_{s-p}^{-1} = \frac{N_L \cdot N_p}{N_s} \tag{23}$$

Box 9

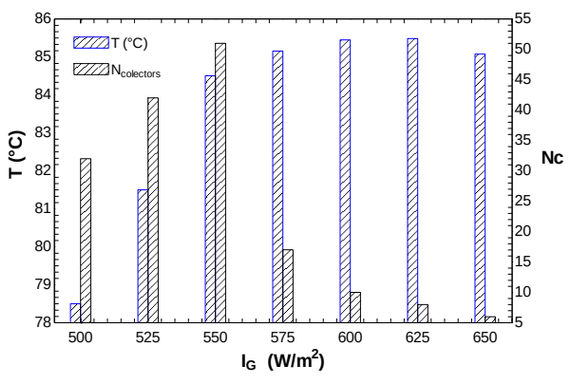

Graph 5

Number of solar collectors in series to reach the objective temperature with respect to solar radiation. T_i=75°C, volumetric flow rate=6.685 l/min.

ISSN: 2524-2121.
RENIECYT-CONAHCYT: 1702902

Lugo-Granados, Hebert Gerardo, Canizalez-Dávalos, Lázaro and Picón-Núñez, Martín. [2024]. Thermoeconomic analysis in solar collector fields: a focus on constant flowrate and variable flowrate models. ECORFAN-Journal Taiwan. 8 [15]1-12: e2815112.
https://doi.org/10.35429/EJT.2024.8.15.1.12

Effect of scaling fouling in the operation models: constant flowrate and variable flowrate

In Graph 6, graphs of the volumetric flow rate necessary to maintain a constant outlet temperature (85°C) are shown with respect to solar time. Environmental conditions change throughout the day, so the flowrate must be adjusted to maintain a constant outlet temperature. As solar time increases, the amount of energy received by the collectors also increases, necessitating flowrate adjustments to maintain the desired outlet temperature, reaching a maximum when solar radiation is highest (see Figure 4).

Under clean conditions (black line, Graph 6), higher flow rates are achieved, resulting in greater thermal load. Over time, the presence of scaling fouling on the collectors (blue and red lines, Graph 2) increases, causing a reduction in the amount of solar energy absorbed. Therefore, volumetric flow rates must be reduced relative to when there is no fouling to maintain the constant outlet temperature.

Box 10

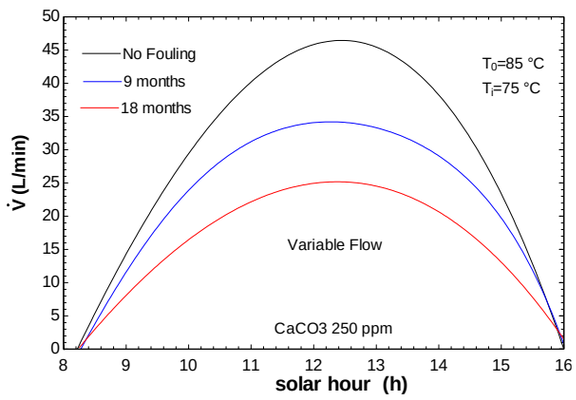

Graph 6

Variation of volumetric flow rate with the day

When operating with variable flowrate, pressure drop varies throughout the solar day (Graph 7).

In the presence of scaling fouling (blue and red lines, Graph 7), pressure drops increase significantly after 18 months of operation due to deposits on the collectors increasing hydraulic resistance.

Box 11

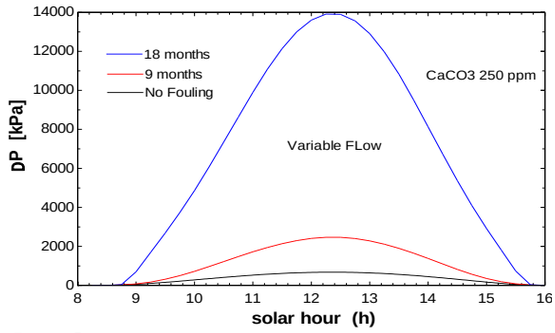

Graph 7

Pressure drop variation during the day for fouling established at different accumulated operation times compared to clean conditions

When operating with constant flowrate, the outlet temperature of solar collectors varies throughout a solar day (see Graph 8). As solar time changes, the outlet temperature in the solar field also adjusts. The highest temperature is obtained at noon when solar radiation is at its maximum. Under clean conditions (black line, Graph 8), a maximum temperature of 114.5°C is reached. After 9 months of operation, the maximum achievable temperature decreases to 113.5°C. When operating for 18 months, the maximum temperature achieved is 112°C.

Box 12

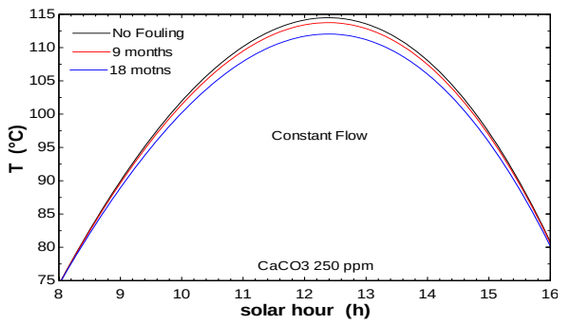

Graph 8

Outlet temperature vs solar time for different volumetric flow rates

In Graph 9, graphs of the thermal load generated by the collectors are shown with respect to solar time when fouling is present for both constant flowrate and variable flowrate models. With the variable flowrate model under clean conditions, the highest instantaneous thermal load is obtained (2,900 kWh). After operating for 9 months, the energy level achieved is 2,100 kWh. At 18 months, the maximum is 1,550 kWh, representing a 46.5% reduction compared to clean conditions.

ISSN: 2524-2121.
RENIECYT-CONAHCYT: 1702902

Lugo-Granados, Hebert Gerardo, Canizalez-Dávalos, Lázaro and Picón-Núñez, Martín. [2024]. Thermoeconomic analysis in solar collector fields: a focus on constant flowrate and variable flowrate models. ECORFAN-Journal Taiwan. 8 [15]1-12: e2815112.
https://doi.org/10.35429/EJT.2024.8.15.1.12

Box 13

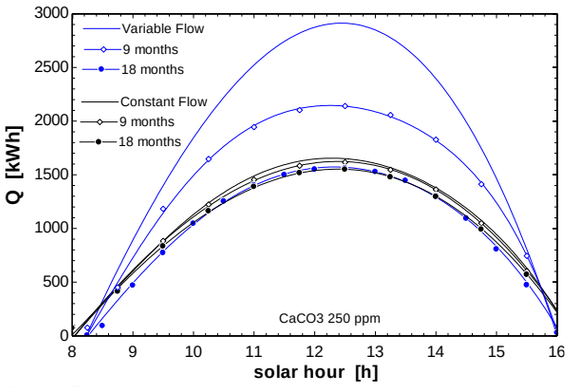

Graph 9

Heat load with respect to solar time for the two models considering fouling

For the constant flowrate model, the maximum instantaneous energy obtained is 1,650 kWh when no fouling is present. After 18 months of operation, the thermal load decreases by 1,000 kWh, representing a 6.5% reduction. These results indicate that scaling fouling has a greater effect on the variable flowrate model.

Cost Analysis

In Tables 2 to 4, the results of the annualised cost analysis for constant flowrate and variable flowrate models are presented under clean conditions and when scaling occurs. The reference case indicates the minimum operating variables required for the process. The flowrate of 6,685 l/min takes 15 minutes to flow through the entire network. Therefore, the analysis was conducted within this time interval.

The inlet temperature is maintained at 75°C. The thermal load and operating costs obtained in each interval are summed to obtain the total. The annualized cost for the 32 collectors is $2,597.65, and this value is added to the pumping cost to obtain the total cost.

The unit cost is obtained by dividing the total cost by the total thermal load.

From the results, it is observed that operating with the variable flowrate model (Table 2) generates the lowest unit cost (0.048 /kWh). The obtained thermal load (59,613.12kWh) exceeds the reference case load by331/kWh. Compared to the reference case, costs are reduced by 61.9%, and 162% more thermal load is produced.

When comparing solar energy usage with natural gas, which has an international price of 0.1 $/kWh, it is found that solar energy has a lower cost.

However, the scaling fouling effect on the collectors must be considered, as their thermohydraulic performance significantly decreases after a period of operation.

Box 14

Table 2

Cost analysis for different modes of operation without fouling

Flowrate (l/min)	ΔP (kPa)	Cost_pump ($)	Cost Total ($)	Q (kWh)	Cost_Q ($/kWh)	T_o (°C)	T_tank (°C)
Reference case							
6.685	14.66	16.08	2,613.72	13,831.93	0.189	85	85
Constant flowrate							
6.685	14.66	16.08	2,613.72	36,239.59	0.072	Variable	101.20
Variable flowrate							
Variable	Variable	297.33	2,894.98	59,613.12	0.048	85	85

After 9 months of operation, considering the presence of scaling-induced fouling (Table 3), using the constant flowrate model results in a temperature drop of 0.5°C in the storage tank.

The thermal load produced decreases by 1.9%, and the unit price increases by 2% compared to when no fouling exists. For the variable flowrate model, the thermal load is reduced by 22%, while the unit cost increases by 44%.

Box 15

Table 3

Cost analysis for different operation modes with fouling (9 months operation)

Flowrate (l/min)	ΔP (kPa)	Cost_pump ($)	Cost Total ($)	Q (kWh)	Cost_Q ($/kWh)	T_o (°C)	T_tank (°C)
Reference case							
6.685	19.56	16.64	2,614.30	13,728.00	0.19	85	85
Constant flowrate							
6.685	Variable	16.62	2,614.26	35,560.89	0.0735	Variable	100.7
Variable flowrate							
Variable	Variable	634.33	3,231.98	46,357.83	0.0697	85	85

When operating with the variable flowrate model for 18 months, from a thermal perspective, it remains profitable, but not economically viable, as the cost increases to 0.154 kWh, which is no longer competitive compared to natural gas usage (0.1 $/kWh). When operating for 18 months with the constant flowrate model, considering scaling presence, the temperature in the storage tank drops by 1.7°C, the thermal load decreases by 6%, and the unit cost increases by 7% compared to clean conditions.

ISSN: 2524-2121.
RENIECYT-CONAHCYT: 1702902

Lugo-Granados, Hebert Gerardo, Canizalez-Dávalos, Lázaro and Picón-Núñez, Martín. [2024]. Thermoeconomic analysis in solar collector fields: a focus on constant flowrate and variable flowrate models. ECORFAN-Journal Taiwan. 8 [15]1-12: e2815112.
https://doi.org/10.35429/EJT.2024.8.15.1.12

Despite this, it remains economically viable in terms of thermal load, although regular cleaning maintenance is necessary.

Box 16

Table 4

Cost analysis for different operation modes with fouling (18 months operation)

Flowrate (l/min)	ΔP (kPa)	Cost_pump ($)	Cost Total ($)	Q (kWh)	Cost_Q ($/kWh)	T_o (°C)	T_tank (°C)
Reference case							
6.685	36.88	$18.67	$2,616.32	13,662.000	$0.191	85	85
Constant flow rate							
6.685	Variable	18.56	2,616.21	33,904.90	0.077	Variable	99.5
Variable flowrate							
Variable	Variable	2,503.64	5,101.29	32,979.48	0.154	85	85

Conclusions

The solar collector's inlet temperature is relatively high at 75°C, requiring elevated radiation (<550 W/m²) to reach the target temperature. With radiation below 600 W/m², 17 collectors are needed to achieve the target temperature (85°C).

Operating above this radiation level reduces the required area by 53%.

Therefore, it is recommended to operate during hours when radiation exceeds 600 W/m² rather than attempting to increase the collection area. However, there is no specific operating schedule for the network.

According to the network design, a configuration of 4 lines with 8 series-connected heat exchangers per line is sufficient to provide the thermal load to the process. It exhibits good thermohydraulic performance according to the series-parallel relationship (Rs-p=2). However, operation should begin when radiation exceeds 600 W/m². With this network configuration, operating with constant flowrate can increase the required thermal load (13,831.93 kWh) by 162% (36,239.59 kWh), while variable flowrate increases it by 331% (59,613.12 kWh).

Under clean conditions, operating with variable flowrate presents better thermoeconomic performance compared to constant flowrate. Without fouling, the variable flowrate model achieves a 64% higher thermal load and 33% lower unit operating costs than the constant flowrate model.

Using solar collectors with a variable flowrate model for pasteurization reduces costs by more than half (0.048 /kWh) compared to natural gas usage (assuming a unit cost of 0.1/kWh). However, the effects of scaling fouling on solar collectors must be considered. If operated without maintenance for 18 months, the cost increases to 0.154 $/kWh.

In the presence of scaling, it is better to operate with constant flowrate since fouling has a lesser impact on the thermoeconomic performance of the collectors. If maximising solar field benefits, operating with constant flowrate and performing cleaning at least once a year is ideal for economic viability.

Declarations

Conflict of interest

The authors declare no interest conflict. They have no known competing financial interests or personal relationships that could have appeared to influence the article reported in this article.

Author contribution

Lugo-Granados, Hebert Gerardo: Contributed to the research methodology and generation of results and writing of the manuscript.

Canizalez-Dávalos, Lázaro: Contributed to the research method and revision of the manuscript.

Picón-Núñez, Martín: Contributed to the project idea, research method, editing and revising of the manuscript.

Funding

This work has been funded by CONAHCYT: the program: Estancia Posdoctoral Académica Inicial 2022(1) [Grant number 2466286, 487049].

Abbreviations

A_c	Collector area 2.506 (m^2)
A_s	Plate area (m^2)
C_1	Ca^{2+} concentration(kg/m^3),
C_2	CO_3^{2-} concentration(kg/m^3)
C_b	Thermal resistance between tube and plate (m^2 °C/W)
$Cost_a$	Annualised cost of solar collector ($/year)

ISSN: 2524-2121.
RENIECYT-CONAHCYT: 1702902

Lugo-Granados, Hebert Gerardo, Canizalez-Dávalos, Lázaro and Picón-Núñez, Martín. [2024]. Thermoeconomic analysis in solar collector fields: a focus on constant flowrate and variable flowrate models. ECORFAN-Journal Taiwan. 8 [15]1-12: e2815112.
https://doi.org/10.35429/EJT.2024.8.15.1.12

$Cost_b$	Operating cost ($)
$Cost_T$	Total operating cost ($)
$cost_u$	Unit cost of electricity ($/kwh)
Cp	Water heat capacity (kJ/kg °C)
C_u	Commercial cost of a solar collector ($811.76 dollars)
d_0	Collector tube outer diameter (m).
d_i	Collector tube inner diameter (m)
d_s	Hydraulic diameter (m)
f	Friction factor
$F´$	Collector efficiency factor
F_A	Metal fin thermal efficiency
Ƒa	Annualization factor
F_R	Heat removal factor
$ï$	Interest rate (8%)
I_G	Solar radiation (W/m^2)
K_1	Friction resistance (kPa s^2/m^6)
K_2	Hydraulic resistance due to connections (kPa s^2/m^6)
k_b	Thermal conductivity (W/m °C)
k_r	Reaction constant (m^2/kg s)
k_f	Resistance factor
K_s	Thermal conductivity of plate (W/m °C)
K_{sp}	$CaCO_3$ solubility (kg^2/m^6)
L_t	Tube length (m)
n	Collector lifespan.
m	Mass deposited in the storage tank each cycle (kg)
mT	Total mass deposited in the storage tank (kg)
$\dot{m}_d$	Mass flux (kg/m^2 s)
$\dot{m}_f$	Mass flow rate (kg/s)
$\dot{m}_r$	Mass flux removed (kg/m^2 s
Nc	Total number of collectors
Q	Process thermal load
Q_u	Useful heat (kW)
Q_T	Total heat load (kW)
Re	Reynolds number
R_h	Thermal resistance due to convection (m^2 °C/W)
R_s	Thermal resistance due to fouling (m^2 °C/W)
R_t	Thermal resistance due to conduction (m2 °C/W),
S	Distance between tubes (m)|
t	Operating time (h).
T_0	Outlet temperature (°C)
T_a	Ambient temperature (°C)
T_i	Inlet temperature (°C)
T_{tank}	Storage tank temperature
T_{pm}	Plate temperature (°C)
U_c	Overall heat transfer coefficient of losses (W/m^2°C)
W	Width (m)
x_f	Fouling layer thickness (m)
$\dot{V}$	Volumetric flow rate (m^3/s)
ΔP	Pressure drop (kPa)
$\dot{w}$	Pumping power

Symbols

α	Deposition resistance factor
α_c	Plate absorbance
β	Mass transfer coefficient (m/s)
γ	Thickness between plate and tube (m)
δ	Plate thickness (m)
εc	Boiler efficiency
η	Collector thermal efficiency
η_b	Pump efficiency
Θ	Cycle iteration
ï	Annual interest rate
λf	Thermal conductivity of $CaCO_3$ (W/m °C)
ρ	Density of water (kg/m^3)
ρf	Density of $CaCO_3$ (kg/m^3)
τ	Cover transmittance
ω	Collector lifespan of 20 years

References

Antecedents

Bunea, M., Eicher, S., Hildbrand, C., Bony, J., Perers, B., Citherlet, S. (2012). Performance of solar collectors under low temperature conditions: Measurements and simulations results. Eurosun, 1-8.

Hanson, M. L., Wendorff, W. L., Houck, K. B. (2005). Effect of Heat Treatment of Milk on Activation of Bacillus Spores. Journal of Food Protection, 1484–1486.

Basics

Dembeck-Kerekes, T., Fine J. P., Friedman J., Dworkin S. B., McArthur J. J. (2019). Performance of Variable Flow Rates for Photovoltaic Thermal Collectors and the Determination of Optimal Flow Rates. Solar Energy, 148-160.

Maroto-Izquierdo, B., Soria Verdugo, A. (2010). P asteurización de leche con Energía solar térmica. Universidad Carlos III de Madrid.

Sokhansefat, T., Kasaeian, A., Rahmani, K., Heidari, A. H, Aghakhani F., Mahian, O. (2018). Thermoeconomic and environmental analysis of solar flat plate and evacuated tube collectors in cold climatic conditions. Renewable Energy, 501-508.

ISSN: 2524-2121.
RENIECYT-CONAHCYT: 1702902

Lugo-Granados, Hebert Gerardo, Canizalez-Dávalos, Lázaro and Picón-Núñez, Martín. [2024]. Thermoeconomic analysis in solar collector fields: a focus on constant flowrate and variable flowrate models. ECORFAN-Journal Taiwan. 8 [15]1-12: e2815112.
https://doi.org/10.35429/EJT.2024.8.15.1.12

Zhuang, Z., Liu, Y., Chen Y., Zhao Y., Wang D., Ma J., Nan, S., (2024). An innovative variable flow control strategy and system performance analysis of a solar collector field. Applied Thermal Engineering, 123753.

Supports

Arunachala, U. C., Bhatt, M. S., Sreepathi, L. K. (2015). Analytical and Experimental Investigation to Determine the Variation of Hottel–Whillier–Bliss Constants for a Scaled Forced Circulation Flat-Plate Solar Water Heater. Sol. Energy Eng, 051011.

Du, B., Lund, P.D., Wang, J. (2022). Improving the accuracy of predicting the performance of solar collectors through clustering analysis with artificial neural network models. Energy Reports, 3970–3981.

Lugo-Granados, H., Picón Núñez M. (2018). Modelling scaling growth in heat transfer surfaces and its application on the design of heat exchangers. Energy, 845-854.

Lugo-Granados, H., Canizalez-Dávalos, L., Picón-Núñez, M. (2023). Thermohydraulic Effects of Scaling in Flat Plate Solar Collector Networks. Chemical Engineering Transactions, 421-426.

Lugo-Granados, H., Canizalez-Dávalos, L., Picón-Núñez, M. (2024). Flat plate solar collector networks: Design and retrofit considering fouling effects. Thermal Science and Engineering Progress, 102633.

Majumdar, R., Sahab, S. K., Patki, A. (2020). Novel dimension scaling for optimal mass flow rate estimation in low temperature flat plate solar collector based on thermal performance parameters. Thermal Science and Engineering Progress, 100569.

Momodu-Bangura, A. B., Hantoro, R., Fudhloli, A., Uwitije, P.D. (2022). Mathematical Model of the Thermal Performance of Double-Pass Solar Collector for Solar Energy Application in Sierra Leone. International Journal of Renewable Energy Development, 347-355.

Quan Z. H., Chen Y. C., Ma C. F. (2008). Heat mass transfer model of fouling process of calcium carbonate on heat transfer surface. Science in China Series Technological Sciences, 882-889.

Unterberger, V., Lichtenegger, K., Kaisermayer, V., Gölles, M., Horn, M. (2021). An adaptive short-term forecasting method for the energy yield of flat-plate solar collector systems. Applied. Energy, 116891.

Wang, D., Zhang, R., Liu, Y., Zhang, X., Fan, J. (2021). Optimization of the flow resistance characteristics of the direct return flat plate solar collector field. Solar Energy. 388–402.

ISSN: 2524-2121.
RENIECYT-CONAHCYT: 1702902

Lugo-Granados, Hebert Gerardo, Canizalez-Dávalos, Lázaro and Picón-Núñez, Martín. [2024]. Thermoeconomic analysis in solar collector fields: a focus on constant flowrate and variable flowrate models. ECORFAN-Journal Taiwan. 8 [15]1-12: e2815112.
https://doi.org/10.35429/EJT.2024.8.15.1.12

ECORFAN-Journal Taiwan 8[15]1-7: e3815107
Article

Construction and development of an ultrasonic spray pyrolysis system for semiconductor thin films deposition to photovoltaic applications

Construcción y desarrollo de un sistema de rocío pirolítico ultrasónico para el depósito de semiconductores en películas delgadas para aplicaciones fotovoltaicas

Palacio-Sifuentes, David *[a], Álvarez-Macias, Carlos [b], Rodríguez-Castro, Sergio[c] and Martínez-López, Ricardo [d]

Tecnológico Nacional de México/Instituto Tecnológico de La Laguna • LDG-3672-2024 • 0009-0009-7454-5808 • 1305504.
Tecnológico Nacional de México/Instituto Tecnológico de La Laguna • H-3977-2017 • 0000-0002-2263-0316 • SNII-CVU:165872
Tecnológico Nacional de México/Instituto Tecnológico de La Laguna • KUD-4774-2024• 0000-0002-6095-2009 • 740722
Tecnológico Nacional de México/Instituto Tecnológico de La Laguna • LDG-7922-2024 • 0009-0004-5606-764X • 325412

CONAHCYT classification:

Area: Engineering
Field: Engineering
Discipline: Electronic Engineering
Subdiscipline: Materials Engineering

https://doi.org/10.35429/EJT.2024.8.15.1.7
History of the article:
Received: February 23, 2024
Accepted: December 06, 2024

* ✉ [m.dipalacios@correo.itlalaguna.edu.mx]

Abstract

The ultrasonic spray pyrolysis (UPS) technique is an efficient method for depositing high-quality thin films, offering advantages over traditional methods. This paper presents the construction and development of a USP system designed for semiconductor thin films used in photovoltaic applications. It provides an overview of the technique, including the setup, material preparation, and process control. The results demonstrate the system's ability to produce uniform, high-quality films, underscoring its potential to advance semiconductor research and inspire new applications in photovoltaics.

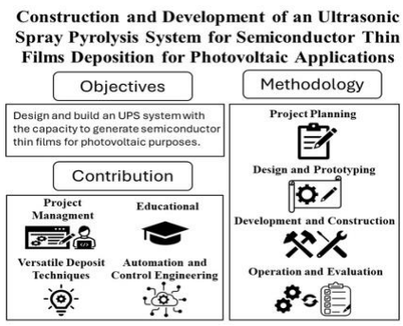

Deposition thecniques, Spray pyrolysis, Thin films

Resumen

La técnica de pirolisis por ultrasonido (USP) es un método eficaz para depositar películas delgadas de alta calidad, con ventajas sobre los métodos tradicionales. Este artículo muestra cómo se construyó y desarrolló un sistema USP para películas delgadas de semiconductores en aplicaciones solares. Se explica de manera sencilla cómo funciona la técnica, desde la preparación de materiales hasta el control del proceso. Los resultados confirman que el sistema puede producir películas uniformes y de buena calidad, lo que lo convierte en una herramienta valiosa para mejorar la investigación en semiconductores.

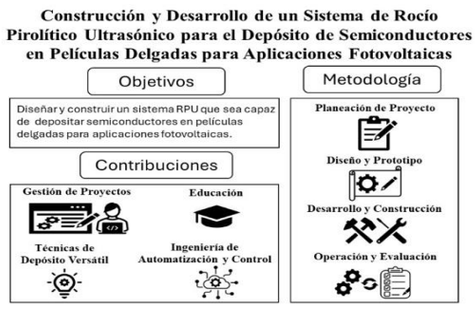

Tecnicas de depocisión, Rocio pirolitico, Laminas delgadas

Citation: Palacio-Sifuentes, David, Álvarez-Macias, Carlos, Rodríguez-Castro, Sergio and Martínez-López, Ricardo. [2024]. Construction and development of an ultrasonic spray pyrolysis system for semiconductor thin films deposition to photovoltaic applications. ECORFAN-Journal Taiwan. 8 [15]1-7: e3815107.

Introduction

Material investigation advancement has focused on semiconductor technology for many decades (Sze, S. M. 2002). Their electrical properties make the semiconductor suitable for energy networks and power electronic applications (Baliga, B. J. 1996). Specifically speaking, these materials play a vital role in the advancement and efficiency of renewable energy technologies. <

Their unique optoelectronic properties are essential in converting and managing energy from renewable sources such as solar (Green, M. A. 2000), wind (Son, J.-Y. et al. 2017), and hydroelectric power (Nababan, S. et al. 2012).

Notably, the photovoltaic field requires semiconductors since these play a crucial role, serving as the foundational materials for solar cells that convert sunlight into electricity. Their unique electrical properties, which allow them to conduct electricity under certain conditions while acting as insulators under others, make them ideal for capturing and converting solar energy efficiently.

Silicon, the most widely used semiconductor in PV cells, has been instrumental in achieving significant improvements in the efficiency and cost-effectiveness of solar panels (Green, M. A. 2005).

Innovations in semiconductor materials and technologies have enabled the development of high-efficiency solar cells, which are essential for increasing the adoption of solar energy (Green, M. A. et al., 2019). By enhancing the performance and reducing the costs of PV technology, semiconductors contribute significantly to the global transition towards sustainable energy sources, helping to mitigate climate change and reduce dependence on fossil fuels.

Unsurprisingly, their development has allowed these materials to go through different manufacturing processes, from their implementation in bulk to their execution in thin films and nanotechnology. Most bulk semiconductors are typically obtained through a series of processes that involve the purification, crystallization, and doping of materials, like silicon, due to its abundance.

However, obtaining semiconductors through thin film deposition techniques has made it possible to generate high-quality materials. These techniques allow precise control over the material's physical properties, such as its thickness, electrical and morphological characteristics, to name a few examples (Chen, Z. et. al. 2012).

Thin film deposition techniques play a critical role in a new generation of solar cells, depositing fragile semiconductor material layers onto a substrate, forming the essential optoelectronic properties (Chopra, K. L. et al. 2004).

There is a wide variety of techniques capable of depositing thin films. Still, the vast majority can be classified as completely chemical, entirely physical, or a combination of both in different stages (Kern, W. et al. 2001). Among the most frequently used deposit techniques are the implementation of Physical Vapor Deposition (PVD), Chemical Vapor Deposition (CVD), and Atomic Layer Deposition (ALD).

These techniques offer distinct advantages and are selected based on the desired material properties and applications.

PVD, including methods like sputtering and evaporation, allows for the deposition of metals, insulators, and semiconductors, providing high-purity films with excellent adhesion and uniformity. On the other hand, CVD is advantageous for its ability to produce high-quality, conformal films over complex geometries, making it ideal for applications in microelectronics and nanotechnology.

ALD stands out for its precision, enabling atomic-level control over film thickness and composition, which is critical for advanced electronic and optical devices (Kern, W. et al. 2001, M. N. Chaudhari 2021). The choice of deposition technique directly influences the thin films' microstructure, crystallinity, and chemical composition, thereby determining their electrical, optical and morphological properties. Furthermore, many of these techniques have modifications or variants in their deposition trajectory, allowing the method to generate specific characteristics in the thin film that may not be visualized in films obtained using the original technique.

ISSN: 2524-2121.
RENIECYT-CONAHCYT: 1702902

Palacio-Sifuentes, David, Álvarez-Macias, Carlos, Rodríguez-Castro, Sergio and Martínez-López, Ricardo. [2024]. Construction and development of an ultrasonic spray pyrolysis system for semiconductor thin films deposition to photovoltaic applications. ECORFAN-Journal Taiwan. 8 [15]1-7: e3815107.
https://doi.org/10.35429/EJT.2024.8.15.1.7

As a result, understanding and selecting the appropriate deposition method is essential for tailoring material characteristics to specific technological applications (Bunshah, R. F. 1982).

Ultrasonic Spray Pyrolysis (USP) is categorized as a vapor chemical technique. It does not require strict growth environments such as low pressures or vacuums, making it a relatively simple and economical technique compared with other physical and chemical methods. Likewise, the USP results in homogeneous growth for forming thin films (Patil, P.S. et al. 1999), converting it into a versatile and attractive technique to produce semiconductor materials.

The USP technique involves producing atomic species, the material to be deposited in a micrometric format (generally droplets), using an ultrasonic nebulizer or atomizer.

The nuclear species generated are transferred with a carrier gas that can be oxygen, nitrogen, argon or another type of gas, depending on what is required to be deposited.

The micrometric droplets collide with the surface where you want to grow the thin film (usually a substrate). The growth environment must be subjected to adequate temperatures provided by a reactor or thermal chamber.

The temperature decomposes the droplets, allowing the thin film to form with the accumulation of particles on the substrate, leaving only the supplied materials that want to be deposited; this is known as pyrolysis (Mwakikunga, B. W. 2013). Figure 1 shows a general diagram of the technique.

Box 1

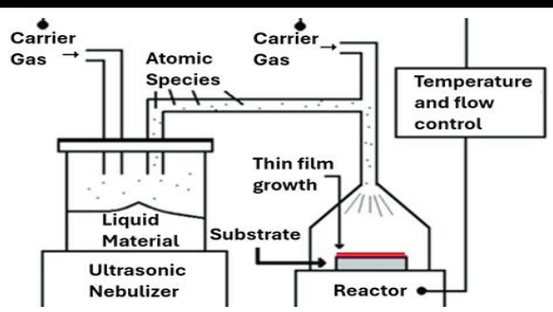

Figure 1

General diagram of the USP technique

Source: Mwakikunga, B. W. 2013

This paper plans to document the construction and development of a USP system capable of depositing semiconductor thin films. The article's structure includes an introduction in section I, the experimental development of the system in section II, the obtained results, and finally, the conclusions for sections III and IV, respectively.

Methodology

The design and construction of the USP system are guided by the diagram presented in Figure 2.

Box 2

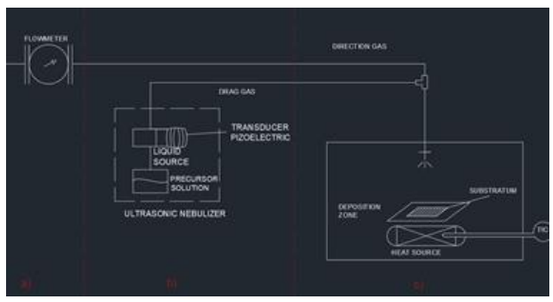

Figure 2

Diagram of USP system made in AutoCAD 3D. Section a) corresponds to the carrier and directional gas distribution and the gas source. Section b) pertains to the ultrasonic nebulization and precursor solution. Section c) covers the deposition area, heat source, and temperature control.

Component Description

This implies the construction and application of specific elements to carry out the technique.

A.- Ultrasonic Nebulizer

A YUE HUA ultrasonic nebulizer WH-2000 model (Figure 3) with an ultrasonic frequency of 1.7 MHz was coupled to the system. This element contains the integrated piezoelectric transducer where the precursor solution is placed once prepared.

The ultrasonic nebulizer is the most significant element of the USP technique; in addition, the magnitude of the frequency allows the size of the droplets to be regulated, improving the deposition of the thin film.

ISSN: 2524-2121.
RENIECYT-CONAHCYT: 1702902

Palacio-Sifuentes, David, Álvarez-Macias, Carlos, Rodríguez-Castro, Sergio and Martínez-López, Ricardo. [2024]. Construction and development of an ultrasonic spray pyrolysis system for semiconductor thin films deposition to photovoltaic applications. ECORFAN-Journal Taiwan. 8 [15]1-7: e3815107.
https://doi.org/10.35429/EJT.2024.8.15.1.7

Box 3

Figura 3

Ultrasonic nebulizer WH-2000 (YUE HUA)

Source: Global Sources Official Website

B.- Reactor Chamber

The reactor is characterized by providing the thermal energy necessary for the pyrolysis process. It is also the instrument where substrates are placed so thin films can be deposited by the atomic species transferred from the nebulizer. For that matter, specific requirements must be formulated.

On the pyrolysis part, it is required for the substrate to be able to vary its temperature, allowing the study and investigation of the temperature influence in thin films (Afify, H.H. et al. 1991). In addition, different materials can be deposited at various temperatures, thus expanding the range of possibilities planned for thin films that are intended to be deposited.

Even so, the USP technique is characterized by maintaining low temperatures compared to other chemical techniques, so handling temperatures of 400 ^{o}C are usually considered high (Patil, P.S. et. al. 1999).

For the place where the substrates are placed inside the reactor, a bowl-type container was sized with measurements of 10 cm as a diameter and depth of 6 cm; this allows several substrates to grow thin film samples with identical deposit conditions and allows the possibility of carrying out destructive-type techniques to analyse specific properties.

Lukoschus et al. consider this requirement, as well as temperature management, to be one of the significant points in generating an efficient system for the deposition of thin films (Lukoschus et al. 2001).

For the heat source, a liquid tin melting system was designed to prevent the Leidenfrost effect, which causes droplets to bounce on the hot surface, returning to the deposition substrate.

A pair of 980W tungsten resistors from ECOGLASS were used to generate sufficient heat for the melting process. These resistors were embedded in a carved refractory brick, mimicking the shape of domestic heaters, to avoid contact with the metal surfaces of the bowl-type container.

Figure 4(a) illustrates the refractory brick designed in Solidworks, while Figure 4(b) shows the physical counterpart and the resistors used.

Box 4

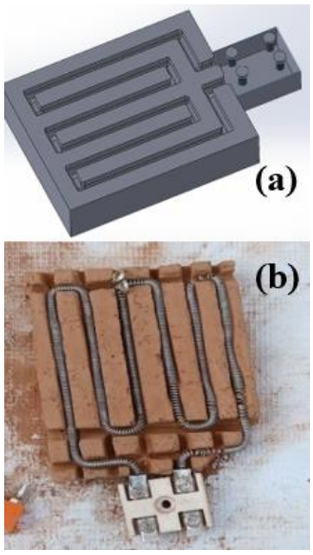

Figure 4

First designed (a) and physical (b) refractory brick

Source: Author

The heat source brick was placed in a heat-resistant stainless-steel box lined inside with a high-temperature ceramic fiber.

A custom-fitted lid with a prepared opening conduit was placed on the metal frame, through which the tin melting process will be carried out inside a small stainless-steel dish (see Figure 5)

ISSN: 2524-2121.
RENIECYT-CONAHCYT: 1702902

Box 5

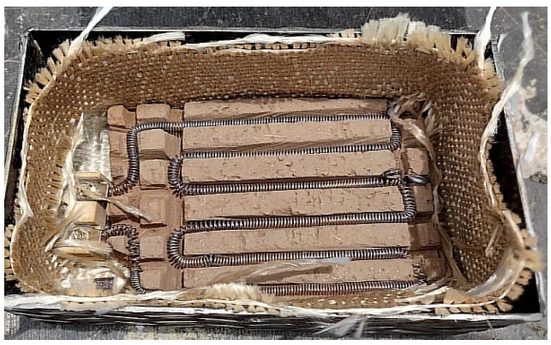

Figure 5
Tin melting prototype
Source: Author

A K thermocouple connected to a PID controller from TECNEU that regulates the current input to the resistances was implemented for the temperature control system.

The entire system was enclosed within an acrylic hood to maintain a closed environment and adapt an extraction system. The final reactor chamber and the interjection pipes of other USP component description areas are shown in Figure 6.

Box 6

Figure 6
Reactor chamber

C.- Carrier gas system

Industrial-grade nitrogen gas was used due to its low reactivity with the chemical components from the precursor substance applied to form thin films.

The gas tank acquired has a pressure regulator used as a flowmeter from WESTON model Z-62900, which allows coordination of the nebula formed by the ultrasonic atomizer, mitigating the turbulence of the deposition velocity in the thin film.

A network of polyurethane pipes was created for the gas transit due to the material's low roughness, preventing turbulence formation within the duct, thus promoting a laminar flow preferred for homogeneous thin film formation.

Results

A prototype of a USP system was built and characterized. The final reactor system consists of three separable modules: The ultrasonic nebulizer, the reactor chamber and the carrier gas system. Figure 7 shows the finalized USP prototype system.

Box 7

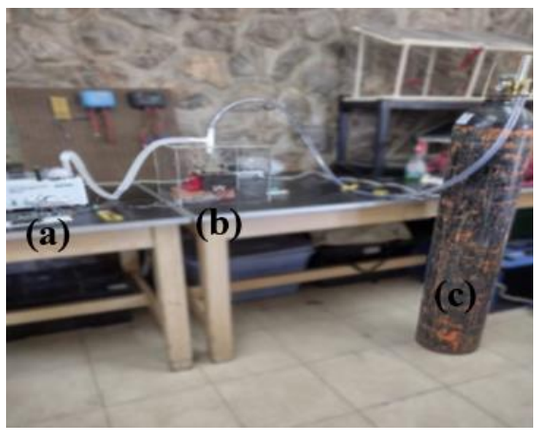

Figure 7
USP prototype system: Ultrasonic nebulizer (a), reactor chamber (b), carrier gas system (c) modules

During preliminary tests, the system achieved temperatures exceeding 300°C, with a peak of 600°C after approximately 15 minutes of exposure.

The use of industrial-grade nitrogen gas for nebulization, along with a network of polyurethane pipes, ensured low reactivity and promoted laminar flow, which is crucial for the formation of high-quality films; this system allows a maximum flow rate of up to 30 liters per minute.

However, for the application of this reactor, flow rate tests were conducted at up to 5 liters per minute, maintaining laminar flow.

Integrating a KJ thermocouple connected to a PID controller allowed precise temperature regulation, contributing to the overall efficiency and reliability of the process.

ISSN: 2524-2121.
RENIECYT-CONAHCYT: 1702902

Palacio-Sifuentes, David, Álvarez-Macias, Carlos, Rodríguez-Castro, Sergio and Martínez-López, Ricardo. [2024]. Construction and development of an ultrasonic spray pyrolysis system for semiconductor thin films deposition to photovoltaic applications. ECORFAN-Journal Taiwan. 8 [15]1-7: e3815107.
https://doi.org/10.35429/EJT.2024.8.15.1.7

The enclosed acrylic hood provided a controlled environment, paving the way for future enhancements with an extraction system. These features collectively contributed to the successful creation of cells within the deposition hood, as evidenced by the stable laminar flow observed during the 10-minute deposition tests.

Conclusions

The construction, development, and implementation of an Ultrasonic Spray Pyrolysis system have been achieved. The system's component integration and preliminary testing have demonstrated significant advancements in the controlled temperature and deposition processes.

The system, composed of three distinct modules, the ultrasonic nebulizer, effectively maintained stable operational conditions for thin film deposition.

Conflict of interest

The authors declare no interest conflict. They have no known competing financial interests or personal relationships that could have appeared to influence the article reported in this document.

Author Contribution

Palacio-Sifuentes, David: Contributed to the project idea, research method and technique, and article writing.

Alvarez-Macias, Carlos: He is Project Leader and Supervisor. He carried out the systematization of the background for the state of the art. He supported the design of the methodology and contributed to the writing of the article.

Rodríguez-Castro, Sergio: contributed to the research of the state of the art, the bibliography and the article's writing.

Martinez-Lopez, Ricardo: contributed to the research design, the type of research, the approach, the method, and the article's writing.

Availability of data and materials:

The data obtained and used in this study are sourced from publicly available articles on the platforms Google Scholar and ResearchGate.

The specific articles that served as information sources can be accessed through relevant searches on these platforms.

Acknowledgment

We thank CONAHCYT [1305504, 2024] and PRODEP [ITLAG-CA-10, 2024]

Abbreviations

ALD	Atomic Layer Deposition
CVD	Chemical Vapor Deposition
PV	Photovoltaic
PVD	Physical Vapor Deposition
USP	Ultrasonic Spray Pyrolysis

References

Background

Sze S. M. [2002] Semiconductor Devices Physics and Technology. USA, John Wiley & Sons, Inc

Baliga, B. J. [1996]. Trends in power semiconductor devices. IEEE Transactions on Electron Devices, 43(10), 1717–1731. DOI: 10.1109/16.536818

Green, M. A. [2000]. Photovoltaics: technology overview. Energy Policy, 28(14), 989–998.

Son, J.-Y. et. al. [2017]. Wind Energy Systems. Proceedings of the IEEE, 105(11), 2116–2131. DOI: 10.1109/JPROC.2017.2695485

Nababan, S. et. al. [2012]. An overview of power topologies for micro-hydro turbines. 2012 3rd IEEE International Symposium on Power Electronics for Distributed Generation Systems (PEDG). DOI: 10.1109/PEDG.2012.6254084

Green, M. A. [2005]. Silicon photovoltaic modules: a brief history of the first 50 years. Progress in Photovoltaics: Research and Applications, 13(5), 447–455. URL.

Basics

Green, M. A. et. al. [2019]. Solar cell efficiency tables (Version 55). Progress in Photovoltaics: Research and Applications, 28(1), 3–15.

ISSN: 2524-2121.
RENIECYT-CONAHCYT: 1702902

Palacio-Sifuentes, David, Álvarez-Macias, Carlos, Rodríguez-Castro, Sergio and Martínez-López, Ricardo. [2024]. Construction and development of an ultrasonic spray pyrolysis system for semiconductor thin films deposition to photovoltaic applications. ECORFAN-Journal Taiwan. 8 [15]1-7: e3815107. https://doi.org/10.35429/EJT.2024.8.15.1.7

Chen, Z. W. et. al. [2011]. Microstructural evolution of oxides and semiconductor thin films. Progress in Materials Science, 56(7), 901–1029.

Chen, Z. et. al. [2012]. Preparation Methodologies and Nano/Microstructural Evaluation of Metal/Semiconductor Thin Films. Journal of Nanoscience and Nanotechnology, 12(1), 26–59.

Support

Chopra, K. L. et. al. [2004]. Thin-film solar cells: an overview. Progress in Photovoltaics: Research and Applications, 12(23), 69–92. DOI: 10.1002/pip.541

Kern, W. et. al. [2001]. Deposition Technologies and Applications. Handbook of Thin Film Deposition Processes and Techniques, 11–43.

Chaudhari M. N. et. al. [2021]. Thin Film Deposition Methods: A Critical Review. Int. J. Res. Appl. Sci. Eng. Technol., 9, 5215.

Differences

Bunshah, R. F. et. al. [1982]. Deposition Technologies for Films and Coatings: Developments and Applications. Noyes Publications, Park Ridge, NJ. URL:

Chaudhari M. N. et. al. [2021]. Thin Film Deposition Methods: A Critical Review. Int. J. Res. Appl. Sci. Eng. Technol., 9, 5215. DOI: 10.22214/ijraset.2021.36154

Patil, P.S. et. al. [1999]. Versatility of chemical spray pyrolysis technique. Mater. Chem. Phys., 59, 185–198.

Disscussion

Mwakikunga, B. W. [2013]. Progress in Ultrasonic Spray Pyrolysis for Condensed Matter Sciences Developed from Ultrasonic Nebulization Theories Since Michael Faraday. Critical Reviews in Solid State and Materials Sciences, 39(1), 46–80.

ISSN: 2524-2121.
RENIECYT-CONAHCYT: 1702902

Palacio-Sifuentes, David, Álvarez-Macias, Carlos, Rodríguez-Castro, Sergio and Martínez-López, Ricardo. [2024]. Construction and development of an ultrasonic spray pyrolysis system for semiconductor thin films deposition to photovoltaic applications. ECORFAN-Journal Taiwan. 8 [15]1-7: e3815107. https://doi.org/10.35429/EJT.2024.8.15.1.7

ECORFAN-Journal Taiwan 8[15]1-7: e4815107
Article

Effect of the angle of solar irradiance on the photo generation of a photovoltaic module

Efecto del ángulo de incidencia solar en la foto generación de un módulo fotovoltaico

Castillo-Campos, Nohemí Alejandra [a], Palacio-Sifuentes, David Isaac [b], Escobedo-Márquez, Diana Laura [c] and Álvarez Macías, Carlos *[d]

[a] Tecnológico Nacional de México/Instituto Tecnológico de La Laguna • LKK-0500-2024 • 0009-0001-2490-4325 • 1271718.
[b] Tecnológico Nacional de México/Instituto Tecnológico de La Laguna • LDG-3672-2024 • 0009-0009-7454-5808 • 1305504.
[c] Tecnológico Nacional de México/Instituto Tecnológico de La Laguna • LKK-0506-2024 • 0009-0005-9859-8251 • 1188232.
[*d] Tecnológico Nacional de México/Instituto Tecnológico de La Laguna • H-3977-2017• 0000-0002-2263-0316 • 165872

CONAHCYT classification:

Area: Engineering
Field: Engineering
Discipline: Energy engineering
Subdiscipline: Solar energy

https://doi.org/10.35429/EJT.2024.8.15.4.7
History of the article:
Received: April 11, 2024
Accepted: December 21, 2024

* ✉ [calvarezm@correo.itlalaguna.edu.mx]

Abstract

The correct installation of a photovoltaic system is vital to obtain the expected generation when sizing the energy that will be needed, since photovoltaic technology is constantly exposed to factors that can reduce its efficiency. In this work, the effect of the angle of solar incidence on the surface of a module was analyzed, through the comparison of the power generated at different angles of inclination from 10 to 45°, and giving the module different angles of orientation from east to west passing through the south (90° to -90° in the azimuth). The behavior of irradiance over time was also analyzed. Derived from this study, it was found that, for the city of Torreon, Coahuila, Mexico photovoltaic modules should be installed facing south and with an inclination of 25°, in addition, the region has an average HSP of 6 hours that occur around noon

Effect of the angle of solar incidence on the photo generation of a photovoltaic module		
Objectives	**Metodology**	**Contribution**
• Analyze the photogeneration of a photovoltaic module according to its inclination and orientation • Check the correct installation parameters for a photovoltaic module in the city of Torreón, Coahuila.	• Evaluation of irradiance reception according to the peak solar hours of the region. • Obtaining efficiency of the module by positioning it with the correct orientation, but varying the inclination. • Analysis of the power loss factor according to the variation of the orientation of the module in the azimuth plane.	The study graphically and mathematically demonstrates the relationship between the orientation and inclination of a photovoltaic module with the energy generation obtained from it, this specifically for the region in which the analysis was carried out.

Photovoltaic energy, Angle incidence, Efficiency

Resumen

La correcta instalación de un sistema fotovoltaico es vital para obtener la generación esperada al momento de dimensionar la energía que se necesitará, esto ya que la tecnología fotovoltaica se expone constantemente a factores que pueden reducir su eficiencia. Es este trabajo se analizó el efecto del ángulo de incidencia solar sobre la superficie de un módulo, a través de la comparación de la potencia generada a distintos ángulos de inclinación de los 10 a 45°, y dando al módulo diferentes ángulos de orientación de es este a oeste pasando por el sur (90° a -90° en el azimut). Así mismo se analizó el comportamiento de la irradiancia en el trascurso del tiempo. Derivado de este estudio se encontró que, para la ciudad de Torreón, Coahuila, México los módulos fotovoltaicos deben instalarse viendo al sur y con una inclinación de 25°, además, la región cuenta con un promedio de HSP de 6 horas que se dan alrededor del mediodía

EFECTO DEL ÁNGULO DE INCIDENCIA SOLAR EN LA FOTO GENERACIÓN UN MÓDULO FOTOVOLTAICO		
Objetivos	**Metodología**	**Contribución**
• Analizar la foto generación de un módulo fotovoltaico de acuerdo a la inclinación y orientación del mismo • Comprobar los parámetros correctos de instalación para un módulo fotovoltaico de la ciudad de Torreón, Coahuila.	• Evaluación de la recepción de irradiancia de acuerdo a las horas solares pico de la región. • Obtención de eficiencia del módulo posicionándolo con la orientación correcta, pero variando la inclinación. • Análisis del factor de perdida de potencia según la variación de la orientación del módulo en el plano azimutal.	El estudio demuestra gráfica y matemáticamente la relación de la orientación y la inclinación de un módulo fotovoltaico con la generación de energía que se obtiene del mismo, esto en especifico para la región en que se realizó el análisis.

Energía fotovoltaica, Ángulo de incidencia, Eficiencia

Citation: Castillo-Campos, Nohemí Alejandra, Palacio-Sifuentes, David Isaac, Escobedo-Márquez, Diana Laura and Álvarez Macías, Carlos. [2024]. Effect of the angle of solar irradiance on the photo generation of a photovoltaic module. ECORFAN-Journal Taiwan. 8 [15]1-7: e4815107.

1. Introduction

Solar irradiance (G), defined as "the radiant flux density of the sun," differs from the radiation emitted by the sun as it is attenuated by the square of the distance between the sun and the surface it reaches. In the case of the irradiance that reaches Earth, the solar constant has been established (Perpignan, 2007).

Although this value may vary depending on the study, the World Meteorological Organization accepts an average value of 1367 W/m². However, this value is reduced by approximately 30% as it passes through the Earth's atmosphere, resulting in a final value of 1 kW/m² (*Perpignan, 2007*).

Due to atmospheric dispersion, global radiation, typically referred to as G_g, is composed of two components: direct radiation (G_b), which originates directly from the solar disk and reaches a specific location, and diffuse radiation (G_d), which is the radiation coming from the entire sky except from the solar disk (*Montoya, 2011*). The expression for global radiation is given in Equation 1.

$$G_g = G_b \times cos\,\theta_z + G_d \quad [1]$$

Where θ_z is the zenith angle θ_z.

Box 1

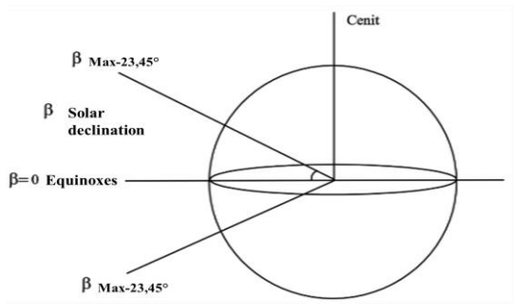

Figure 1

Angles that refer to the position of the sun with respect to apparent motion

The irradiance received at a point on a surface depends on what is known in solarimetry as the apparent motion of the sun, which is influenced by parameters such as the day of the year, time of day, and the sun's position. The sun's path is described by two angles: the zenith angle and the azimuth angle, both illustrated in Figure 1.

The zenith angle θ_z measures how far the sun is from the vertical at any given time, while the azimuth angle γ_s measures the sun's deviation from true south (*Marcial, 2019*).

In addition to the zenith and azimuth angles, another angle often used in solarimetry is the solar height or elevation angle. This angle measures the deviation of the sun from the horizontal, indicating its elevation in the sky.

The solar height angle is complementary to the zenith angle, meaning their sum equals 90°, as shown in Equation 2 (*Marcial, 2019*).

$$\theta_z + \alpha_s = 90° \quad [2]$$

The angle formed between the Earth's equator and the ecliptic is 23° 16' 30", which causes the sun's trajectory to change throughout the year. This variation gives rise to the solar declination angle, δ\deltaδ, defined as the "angle formed by the direction of the sun's rays with the plane of the equator" (*Rodríguez et al, 2022*).

The solar declination can be calculated daily with reasonable accuracy using Equation 3.

$$\delta = 23.45° \; sin\; sin\left[\left(\frac{360°}{365}\right)(284 + N)\right] \quad [3]$$

Where N represents the day of the year. This equation reflects that, throughout the year, the irradiance received on a surface change continuously.

The solar incidence angle refers to the angle at which sunlight strikes a surface. Based on the apparent motion of the sun, it follows that when the sun is near the zenith, the surface tends to receive a greater amount of energy.

This occurs because the path traveled by the sun's rays is shorter when the sun is at its maximum elevation, as shown in Figure 2, where distances X are longer than distance Y.

From this concept arises irradiation, which is the total irradiance received by a surface over a specific period of time. The hours of the day with the highest irradiance are referred to as Peak Sun Hours (PSH) (*Style, 2012*).

ISSN: 2524-2121.
RENIECYT-CONAHCYT: 1702902

Castillo-Campos, Nohemí Alejandra, Palacio-Sifuentes, David Isaac, Escobedo-Márquez, Diana Laura and Álvarez Macías, Carlos. [2024]. Effect of the angle of solar irradiance on the photo generation of a photovoltaic module. ECORFAN-Journal Taiwan. 8 [15]1-7: e4815107.
https://doi.org/10.35429/EJT.2024.8.15.4.7

The performance of a photovoltaic module is directly proportional to the amount of sunlight it receives and its technological ability to convert it into usable energy. The higher the irradiance, the greater the short-circuit current, and vice versa. For this reason, a panel's performance is influenced by various factors, such as the time of year, the day, the region, and its geographical location (*Al Shehri et al, 2016*).

Box 2

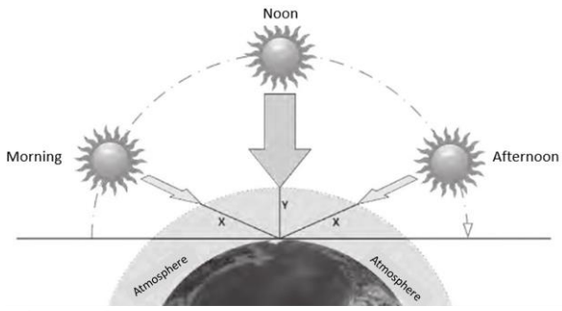

Figure 2
Variation in irradiance during the day
Source: Style, 2012

The optimal orientation for achieving the best performance of a photovoltaic installation is facing south when the location is in the northern hemisphere. Conversely, the panels should be oriented north when the installation is in the southern hemisphere.

For optimal tilt, the inclination should match the latitude of the installation site, which corresponds to the position of the area relative to the equator (north or south). To achieve this, the modules must be adjusted using the appropriate instruments (*Carta et al, 2009*).

A well-planned positioning involves placing the photovoltaic panel in a shadow-free area, orienting it toward the geographic south (or north in the southern hemisphere), and setting it at the appropriate inclination. To ensure that nearby objects do not cast shadows on the panel, it is essential to accurately calculate the lengths and directions of shadows. These calculations should be made with the winter solstice in mind, as this is the day when shadows are at their longest due to the sun's lowest path in the sky (*Carta et al, 2009*).

This work is divided into four sections. The first section provides a brief introduction, outlining the theoretical concepts relevant to the study.

Section 2 explains the methodology, detailing the equipment and procedures used in the experimental process, as well as specifying the techniques employed for measurement collection.

Section 3 presents the results of the analysis, illustrating the effects of solar incidence variation on the surface of the photovoltaic module. Finally, Section 4 includes the study's conclusions and inferences regarding the power generated by the module under different test conditions.

2. Methodology

The development of this experiment was carried out using a 410 W JaSolar photovoltaic module model JAM72S10 410/MR. A sensitive pyranometer (Kipp & Zonen) and a handheld pyranometer (Tenmars) were used for irradiance measurements. The measurement of the module's electrical parameters was carried out with a multimeter for solar panels.

This experiment was conducted using a 410 W JaSolar photovoltaic module, model JAM72S10 410/MR. For irradiance measurements, a sensitive pyranometer (Kipp & Zonen) and a handheld pyranometer (Tenmars) were employed. The electrical parameters of the module were measured using a multimeter specifically designed for solar panels.

To begin the experimental process, a large, shadow-free area was selected. The average irradiation for the region was then identified using the NASA Power platform, which provided the average Peak Sun Hours (PSH) for the city of Torreón, Coah. Figure 3 shows the location of the city on the map (25.54389°, -103.41898°), while Figure 4 displays the results obtained, highlighting the annual average PSH (6.34 hours).

Box 3

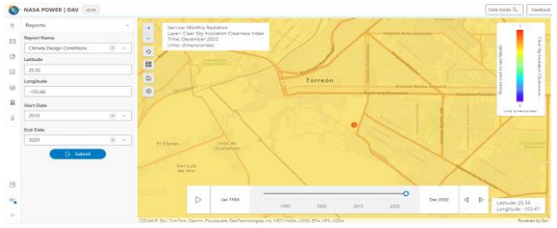

Figure 3
Location of Torreón, Coahuila
https://power.larc.nasa.gov

ISSN: 2524-2121.
RENIECYT-CONAHCYT: 1702902

Castillo-Campos, Nohemí Alejandra, Palacio-Sifuentes, David Isaac, Escobedo-Márquez, Diana Laura and Álvarez Macías, Carlos. [2024]. Effect of the angle of solar irradiance on the photo generation of a photovoltaic module. ECORFAN-Journal Taiwan. 8 [15]1-7: e4815107.
https://doi.org/10.35429/EJT.2024.8.15.4.7

Box 4

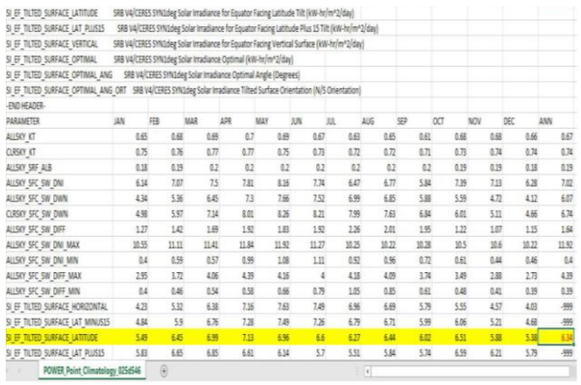

PARAMETER	JAN	FEB	MAR	APR	MAY	JUN	JUL	AUG	SEP	OCT	NOV	DEC	ANN
ALLSKY_KT	0.65	0.68	0.69	0.7	0.69	0.67	0.63	0.65	0.61	0.66	0.66	0.66	0.67
CLRSKY_KT	0.75	0.76	0.77	0.77	0.75	0.73	0.72	0.72	0.71	0.73	0.74	0.74	0.74
ALLSKY_SRF_ALB	0.18	0.19	0.2	0.2	0.2	0.2	0.2	0.2	0.2	0.19	0.19	0.18	0.19
ALLSKY_SFC_SW_DNI	6.14	7.07	7.5	7.81	8.16	7.74	6.47	6.77	5.84	7.39	7.13	6.28	7.02
ALLSKY_SFC_SW_DWN	4.34	5.36	6.45	7.3	7.66	7.52	6.99	6.85	5.88	5.59	4.72	4.12	6.07
CLRSKY_SFC_SW_DWN	4.98	5.97	7.14	8.01	8.26	8.21	7.99	7.83	6.84	6.01	5.11	4.66	6.74
ALLSKY_SFC_SW_DIFF	1.27	1.42	1.69	1.92	1.83	1.92	2.26	2.01	1.95	1.22	1.07	1.15	1.64
ALLSKY_SFC_SW_DNI_MAX	10.55	11.11	11.41	11.84	11.92	11.27	10.25	10.22	10.28	10.5	10.6	10.22	11.92
ALLSKY_SFC_SW_DNI_MIN	0.4	0.59	0.57	0.99	1.08	1.11	0.92	0.96	0.72	0.61	0.44	0.46	0.4
ALLSKY_SFC_SW_DIFF_MAX	2.95	3.72	4.06	4.39	4.16	4	4.18	4.09	3.74	3.49	2.88	2.73	4.39
ALLSKY_SFC_SW_DIFF_MIN	0.4	0.48	0.54	0.58	0.66	0.79	1.05	0.85	0.61	0.48	0.41	0.39	0.39
SI_EF_TILTED_SURFACE_HORIZONTAL	4.23	5.32	6.38	7.16	7.63	7.49	6.96	6.69	5.79	5.55	4.57	4.03	-999
SI_EF_TILTED_SURFACE_LAT_MINUS15	4.84	5.9	6.76	7.28	7.49	7.26	6.79	6.71	5.99	6.06	5.21	4.68	-999
SI_EF_TILTED_SURFACE_LATITUDE	5.49	6.45	6.99	7.13	6.96	6.6	6.27	6.44	6.02	6.51	5.88	5.38	6.34
SI_EF_TILTED_SURFACE_LAT_PLUS15	5.83	6.65	6.85	6.61	6.14	5.7	5.51	5.84	5.74	6.59	6.21	5.79	-999

Figure 4

Annual average of HSP in Torreón, Coahuila

https://power.larc.nasa.gov

Once the average PSH was determined, the first test involved measuring the irradiance in the area over time using both the sensitive pyranometer and the handheld pyranometer, as illustrated in Figure 5.

Box 5

Figure 5

Measurement of irradiance with sensitive pyranometer (Kipp & Zonen) and handheld pyranometer (Tenmars)

For the second test, the module's performance was analyzed based on its installation angle.

The photovoltaic module was oriented south, and its maximum power point was measured while varying the inclination angle from 10° to 45° in 5° intervals.

Figure 6 shows the module facing south at a 25° inclination, which corresponds to the latitude of the region.

Box 6

Figure 6

Location of the module in the photovoltaic test area

To evaluate the module's performance based on its orientation, the final test involved marking out a semicircular area, with angles in the azimuth plane ranging from east to west, passing through the south, in 15° intervals. This setup is shown in Figure 7.

Box 7

Figure 7

Marking of the azimuth plane

Finally, measurements of the module's electrical parameters were taken by varying both the inclination angle and its orientation in the azimuth plane.

This was made possible by using a structure specifically adapted to allow adjustments in both planes.

3. Results

In the first test, the curves obtained from measurements taken with each pyranometer were compared.

This comparison is illustrated in Graph 1, where "Pyranometer 1" refers to the Tenmars handheld pyranometer and "Pyranometer 2" refers to the sensitive Kipp & Zonen pyranometer.

ISSN: 2524-2121.
RENIECYT-CONAHCYT: 1702902

Castillo-Campos, Nohemí Alejandra, Palacio-Sifuentes, David Isaac, Escobedo-Márquez, Diana Laura and Álvarez Macías, Carlos. [2024]. Effect of the angle of solar irradiance on the photo generation of a photovoltaic module. ECORFAN-Journal Taiwan. 8 [15]1-7: e4815107.
https://doi.org/10.35429/EJT.2024.8.15.4.7

Box 8

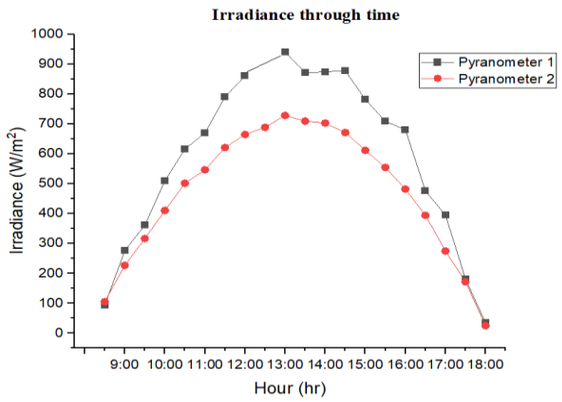

Graph 1

Irradiance over time

The difference in irradiance measurements between the two pyranometers is significant, as Pyranometer 1 has a sensitivity of 10 mW, while Pyranometer 2 has a sensitivity of 10 µW. However, the trends of the curves are consistent, indicating that around noon, which is typically close to the zenith, the highest levels of irradiance are recorded.

This observation confirms that peak solar hours occur around noon, when the sun's rays travel the shortest distance to reach the surface. In both cases, irradiance measurements exceeding 700 W/m² were obtained.

To understand the effect of the angle of solar incidence on the surface of the photovoltaic module, Graph 2 illustrates the efficiency generated by the module at various inclination angles.

Box 8

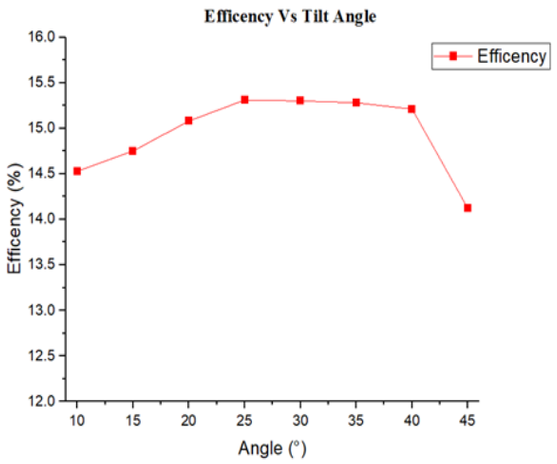

Graph 2

Efficiency of the module against the angle of inclination

From Graph 2, it can be observed that the highest efficiency from the module occurs at inclination angles between 25° and 35°. This aligns with the latitude of the test area, which is 25°. If the module's inclination is adjusted by more than 10° from this range, a decrease in photo generation occurs due to the adverse effects on the angle of solar incidence.

Similarly, Graph 3 illustrates the behavior of the short-circuit current (Isc) generated by the module in relation to the inclination angle, while the module received an average irradiance of 874 W/m².

Box 9

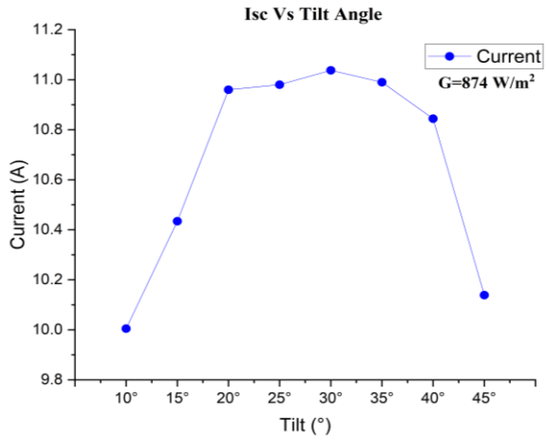

Graph 3

Short circuit current of the module against the angle of inclination

The generation of the short-circuit current in photovoltaic technology is directly dependent on the irradiance received by the PV modules on their surface; the greater the irradiance, the higher the current generated. In Figure 3, it is evident that the highest short-circuit current values occur at inclination angles between 20° and 35°.

In contrast, at other inclination angles, the short-circuit current decreases significantly. This phenomenon occurs because inclinations closer to the region's latitude enhance the reception of direct irradiance, allowing for more effective conversion of solar energy into electrical energy.

Through the third test, Table 1 presents the values of the maximum power point of the module at various orientations in the azimuth plane and different inclination angles.

ISSN: 2524-2121.
RENIECYT-CONAHCYT: 1702902

Castillo-Campos, Nohemí Alejandra, Palacio-Sifuentes, David Isaac, Escobedo-Márquez, Diana Laura and Álvarez Macías, Carlos. [2024]. Effect of the angle of solar irradiance on the photo generation of a photovoltaic module. ECORFAN-Journal Taiwan. 8 [15]1-7: e4815107.
https://doi.org/10.35429/EJT.2024.8.15.4.7

Box 10

Table 1

Power of the module according to orientation

(°)	Inclination							
γ_s	10	15	20	25	30	35	40	45
90	140	195	213	256	244	277	222	138
75	168	254	255	284	268	252	243	192
60	225	267	276	309	292	286	267	262
45	240	268	290	332	323	308	293	263
30	248	280	298	341	326	315	299	280
15	272	282	307	362	336	324	307	287
0	289	310	321	378	367	328	311	299
-15	183	231	282	351	321	313	307	229
-30	136	212	276	344	319	302	297	220
-45	156	165	228	325	311	267	252	145
-60	140	161	218	304	288	232	224	130
-75	94	135	213	289	268	202	152	89
-90	77	129	139	248	224	144	123	50

Source: Own elaboration

Table 1 highlights the value of 378 W, the maximum power output obtained from all measurements, achieved at an inclination of 25° with a direct orientation to the south (0° in the azimuth plane). This result confirms that this orientation is optimal for the region, as it aligns with the correct positioning for solar modules in the northern hemisphere.

Using the values in Table 1, it is possible to calculate the power loss factor corresponding to each orientation and inclination. The loss factor is determined using Equation 4.

$$Loss\ factor = \frac{Generated\ power}{Highest\ power\ measured} * 100 \qquad [4]$$

Table 2 shows the loss factor obtained for each measurement.

Box 11

Table 2

Loss factor according to orientation

(°)	Inclination							
γ_s	10	15	20	25	30	35	40	45
90	-6.2	-4.8	-4.3	-3.2	-3.5	-3.9	-4.1	-6.3
75	-5.5	-3.2	-3.2	-2.4	-2.9	-3.3	-3.5	-4.9
60	-4.0	-2.9	-2.6	-1.8	-2.2	-2.4	-2.9	-3.0
45	-3.6	-2.9	-2.3	-1.2	-1.4	-1.8	-2.2	-3.0
30	-3.4	-2.5	-2.1	-0.9	-1.3	-1.6	-2.0	-2.5
15	-2.7	-2.5	-1.8	-0.4	-1.1	-1.4	-1.8	-2.3
0	-2.3	-1.8	-1.5	0.0	-0.2	-1.3	-1.7	-2.0
-15	-5.1	-3.8	-2.5	-0.7	-1.4	-1.7	-1.8	-3.9
-30	-5.6	-4.3	-2.7	-0.9	-1.5	-2.0	-2.1	-4.1
-45	-5.8	-5.6	-3.9	-1.4	-1.7	-2.9	-3.3	-6.1
-60	-6.2	-5.7	-4.2	-1.9	-2.3	-3.8	-4.0	-6.5
-75	-7.4	-6.4	-4.3	-2.3	-2.9	-4.6	-5.9	-7.6
-90	-7.9	-6.5	-6.3	-3.4	-4.0	-6.1	-6.7	-8.6

Source: Own elaboration

Table 2 illustrates that to minimize the loss factor, the module should be oriented as closely to the south as possible, ideally within the range of -30° to +30°. Additionally, the inclination of the module should be maintained between 25° and 35°. Deviations from these angles tend to result in a higher power loss factor for the module.

4. Conclusions

In this work, research was carried out on the impact of the angle of solar incidence on the electrical parameters of a photovoltaic module. Through the analysis conducted, it was demonstrated that the optimal orientation of a photovoltaic module in the city of Torreón, Coahuila, is southward at 0° in the azimuth plane, with an inclination of 25°.

This configuration allows the surface of the PV module to align as closely as possible with the angle of solar incidence, thereby maximizing efficiency during peak solar hours, which occur around noon, with an average of 6.34 hours of peak sun.

The lowest power loss factor recorded was 0% at 25° inclination and 0° orientation, while the highest loss factor of -8.6% was observed at 45° inclination and -90° orientation.

This research can serve as a reference for other installations where the modules may not be positioned under the ideal conditions, providing insights into optimizing their performance even when perfect alignment is not achievable.

Declarations

Conflict of interest

The authors declare no interest conflict. They have no known competing financial interests or personal relationships that could have appeared to influence the article reported in this article.

Author Contribution

Castillo-Campos, Nohemí Alejandra: She contributed whit the project idea, bibliographic research, data collection and article writing.

Palacio-Sifuentes, David: He carried out the research method and technique, data collection and writing of the article.

ISSN: 2524-2121.
RENIECYT-CONAHCYT: 1702902

Castillo-Campos, Nohemí Alejandra, Palacio-Sifuentes, David Isaac, Escobedo-Márquez, Diana Laura and Álvarez Macías, Carlos. [2024]. Effect of the angle of solar irradiance on the photo generation of a photovoltaic module. ECORFAN-Journal Taiwan. 8 [15]1-7: e4815107.
https://doi.org/10.35429/EJT.2024.8.15.4.7

Escobedo-Marquez, Diana Laura: She contributed whit bibliographic research and article writing.

Alvarez-Macias, Carlos: He contributed to the supervision of the project, as well as the review and editing of the writing and verification of bibliography.

Availability of data and materials

The Hour Solar Pick of any region can be consulted at the NASA's web page; https://power.larc.nasa.gov/data-access-viewer/.

Funding

This work has been funded by CONAHCYT 1271718, 1305504 and 1188232; PRODEP 1188232.

Acknowledgements

The authors thank the support of CONAHCYT 1271718, 1305504 and 1188232; PRODEP 1188232.

Abbreviations

A	Amperes
G	Irradiance
HSP	Hour Solar Pick
I	Current
μW	Microwatts
mW	Milliwatts
Isc	Short Circuit Current
NASA	National Aeronautics and Space Administration
PV	Photovoltaic
W	Watts

References

Antecedents

Al Shehri A, Parrott B, Carrasco P, Al Saiari H, Taie I., "Impact of dust deposition and brush-based dry cleaning on glass transmittance for PV modules applications," Solar Energy, vol. 135, pp. 317-324, 2016.

Basics

Perpiñan Lamigueiro, O. (2007). Solar Radiation. In Photovoltaic solar energy, (Vol. 1, pp. 25–26). essay, Creative commons.

Montoya Rasero, C. (2011). Solar resource. In Photovoltaic Solar Energy (pp. 31–35). essay, School of Industrial Organization.

Marcial Alarcón, A. (2019). Solar Resource. In Photovoltaic Solar Energy (1st ed., pp. 12–13). essay, Elearning S. L.

Rodríguez Mas, F., Ruiz Gómez, A., & Valiente García, D. (2022). Solar radiation. In Notes on photovoltaic energy (p. 22). essay, Miguel Hernández University of Elche.

Style, O. (2012). The sun. In Autonomous Solar Energy: Planning, Dimensioning and Installation of an Autonomous Photovoltaic System (1st ed., pp. 15–16). essay, Ithaca.

Supports

Carta Gonzalez, J. A., Calero Pérez R., Colmenar Santos A., Castro Gil M-A. (2009). "Photovoltaic Solar Power Plants". In Centrales de Energías Renovables (pp. 248-255). essay, Pearson Education.

ISSN: 2524-2121.
RENIECYT-CONAHCYT: 1702902

Castillo-Campos, Nohemí Alejandra, Palacio-Sifuentes, David Isaac, Escobedo-Márquez, Diana Laura and Álvarez Macías, Carlos. [2024]. Effect of the angle of solar irradiance on the photo generation of a photovoltaic module. ECORFAN-Journal Taiwan. 8 [15]1-7: e4815107. https://doi.org/10.35429/EJT.2024.8.15.4.7

[[Title in TNRoman and Bold No. 14 in English and Spanish]

Surname, Name 1st Author*[a], Surname, Name 1st Co-author[b], Surname, Name 2nd Co-author[c] and Surname, Name 3rd Co-author[d] [No.12 TNRoman]

[a] Affiliation institution, Researcher ID, ORC ID, SNI-CONAHCYT ID or CVU PNPC [No.10 TNRoman]
[b] Affiliation institution, Researcher ID, ORC ID, SNI-CONAHCYT ID or CVU PNPC [No.10 TNRoman]
[c] Affiliation institution, Researcher ID, ORC ID, SNI-CONAHCYT ID or CVU PNPC [No.10 TNRoman]
[d] Affiliation institution, Researcher ID, ORC ID, SNI-CONAHCYT ID or CVU PNPC [No.10 TNRoman]

All ROR-Clarivate-ORCID and CONAHCYT profiles must be hyperlinked to your website.
Prot- University of South Australia • 7038-2013• 0000-0001-6442-4409 • 416112

CONAHCYT classification:
https://marvid.org/research_areas.php [No.10 TNRoman]
Area:
Field:
Discipline:
Subdiscipline:

DOI: https://doi.org/
Article History:
Received: [Use Only ECORFAN]
Accepted: [Use Only ECORFAN]
Contact e-mail address:
* ✉ [example@example.org]

Abstract [In English]
Must contain up to 150 words
Graphical abstract [In English]

Authors must provide an original image that clearly represents the article described in the article. Graphical abstracts should be submitted as a separate file. Please note that, as well as each article must be unique. File type: the file types are MS Office files.No additional text, outline or synopsis should be included. Any text or captions must be part of the image file. Do not use unnecessary white space or a "graphic abstract" header within the image file.

Keywords [In English]
Indicate 3 keywords in TNRoman and Bold No. 10

Abstract [In Spanish]
Must contain up to 150 words
Graphical abstract [In Spanish]

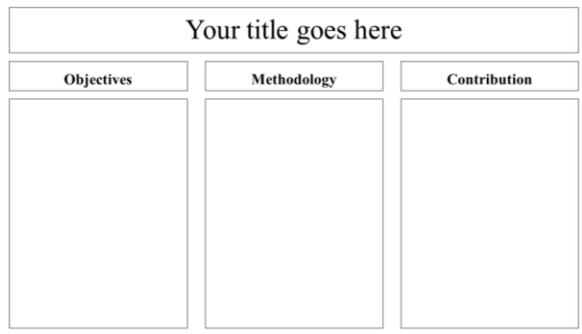

Authors must provide an original image that clearly represents the article described in the article. Graphical abstracts should be submitted as a separate file. Please note that, as well as each article must be unique. File type: the file types are MS Office files.No additional text, outline or synopsis should be included. Any text or captions must be part of the image file. Do not use unnecessary white space or a "graphic abstract" header within the image file.

Keywords [In Spanish]
Indicate 3 keywords in TNRoman and Bold No. 10

Citation: Surname, Name 1st Author, Surname, Name 1st Co-author, Surname, Name 2nd Co-author and Surname, Name 3rd Co-author. Article Title. ECORFAN Journal-Mexico. Year. V-N: Pages [TN Roman No.10].

Introduction

Text in TNRoman No.12, single space.

General explanation of the subject and explain why it is important.

What is your added value with respect to other techniques?

Clearly focus each of its features.

Clearly explain the problem to be solved and the central hypothesis.

Explanation of sections Article.

Development of headings and subheadings of the article with subsequent numbers

[Title No.12 in TNRoman, single spaced and bold]

Products in development No.12 TNRoman, single spaced.

Including figures and tables-Editable

In the article content any table and figure should be editable formats that can change size, type and number of letter, for the purposes of edition, these must be high quality, not pixelated and should be noticeable even reducing image scale.

[Indicating the title at the bottom with No.10 and Times New Roman Bold]

Box

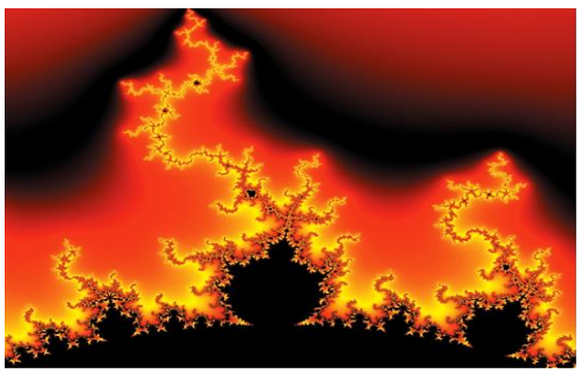

Figure 1

Title [Should not be images-everything must be editable]

Source [in italic]

Box

Table 1

Title [Should not be images-everything must be editable]

Source [in italic]

The maximum number of Boxes is 10 items

For the use of equations, noted as follows:

$$Y_{ij} = \alpha + \sum_{h=1}^{r} \beta_h X_{hij} + u_j + e_{ij} \quad [1]$$

Must be editable and number aligned on the right side.

Methodology

Develop give the meaning of the variables in linear writing and important is the comparison of the used criteria.

Results

The results shall be by section of the article.

Conclusions

Clearly explain the results and possibilities of improvement.

Annexes

Tables and adequate sources.

The international standard is 7 pages minimum and 14 pages maximum.

Declarations

Conflict of interest

The authors declare no interest conflict. They have no known competing financial interests or personal relationships that could have appeared to influence the article reported in this article.

ISSN: 2524-2121.
RENIECYT-CONAHCYT: 1702902

Author contribution

Specify the contribution of each researcher in each of the points developed in this research.

Prot-
Benoit-Pauleter, Gerard: Contributed to the project idea, research method and technique.

Availability of data and materials

Indicate the availability of the data obtained in this research.

Funding

Indicate if the research received some financing.

Acknowledgements

Indicate if they were financed by any institution, University or company.

Abbreviations

List abbreviations in alphabetical order.

Prot-

ANN	Artificial Neural Network

References

Use APA system. Should not be numbered, nor with bullets, however if necessary numbering will be because reference or mention is made somewhere in the Article.

Use the Roman alphabet, all references you have used should be in Roman alphabet, even if you have cited an article, book in any of the official languages of the United Nations [English, French, German, Chinese, Russian, Portuguese, Italian, Spanish, Arabic], you should write the reference in Roman alphabet and not in any of the official languages.

Citations are classified the following categories:

Antecedents. The citation is due to previously published research and orients the citing document within a particular scholarly area.

Basics. The citation is intended to report data sets, methods, concepts and ideas on which the authors of the citing document base their work.

Supports. The citing article reports similar results. It may also refer to similarities in methodology or, in some cases, to the reproduction of results.

Differences. The citing document reports by means of a citation that it has obtained different results to those obtained in the cited document. This may also refer to differences in methodology or differences in sample sizes that affect the results.

Discussions. The citing article cites another study because it is providing a more detailed discussion of the subject matter.

The URL of the resource is activated in the DOI or in the title of the resource.

Prot-
Mandelbrot, B. B. [2020]. Negative dimensions and Hölders, multifractals and their Hölder spectra, and the role of lateral preasymptotics in science. Journal of Fourier Analysis and Applications Special. 409-432.

Intellectual Property Requirements for editing:

- Authentic Signature in Color of Originality Format Author and Coauthors.
- Authentic Signature in Color of the Acceptance Format of Author and Coauthors.
- Authentic Signature in blue color of the Conflict of Interest Format of Author and Co-authors.

ISSN: 2524-2121.
RENIECYT-CONAHCYT: 1702902

Reservation to Editorial Policy

ECORFAN Journal-Taiwan reserves the right to make editorial changes required to adapt the Articles to the Editorial Policy of the Journal. Once the Article is accepted in its final version, the Journal will send the author the proofs for review. ECORFAN® will only accept the correction of errata and errors or omissions arising from the editing process of the Journal, reserving in full the copyrights and content dissemination. No deletions, substitutions or additions that alter the formation of the Article will be accepted.

Code of Ethics - Good Practices and Declaration of Solution to Editorial Conflicts

Declaration of Originality and unpublished character of the Article, of Authors, on the obtaining of data and interpretation of results, Acknowledgments, Conflict of interests, Assignment of rights and Distribution.

The ECORFAN-Mexico, S.C Management claims to Authors of Articles that its content must be original, unpublished and of Scientific, Technological and Innovation content to be submitted for evaluation.

The Authors signing the Article must be the same that have contributed to its conception, realization and development, as well as obtaining the data, interpreting the results, drafting and reviewing it. The Corresponding Author of the proposed Article will request the form that follows.

Article title:

– The sending of an Article to ECORFAN Journal- Taiwan emanates the commitment of the author not to submit it simultaneously to the consideration of other series publications for it must complement the Format of Originality for its Article, unless it is rejected by the Arbitration Committee, it may be withdrawn.

– None of the data presented in this article has been plagiarized or invented. The original data are clearly distinguished from those already published. And it is known of the test in PLAGSCAN if a level of plagiarism is detected Positive will not proceed to arbitrate.

– References are cited on which the information contained in the Article is based, as well as theories and data from other previously published Articles.

– The authors sign the Format of Authorization for their Article to be disseminated by means that ECORFAN-Mexico, S.C. In its Holding Taiwan considers pertinent for disclosure and diffusion of its Article its Rights of Work.

– Consent has been obtained from those who have contributed unpublished data obtained through verbal or written communication, and such communication and Authorship are adequately identified.

– The Author and Co-Authors who sign this work have participated in its planning, design and execution, as well as in the interpretation of the results. They also critically reviewed the paper, approved its final version and agreed with its publication.

– No signature responsible for the work has been omitted and the criteria of Scientific Authorization are satisfied.

– The results of this Article have been interpreted objectively. Any results contrary to the point of view of those who sign are exposed and discussed in the Article.

Copyright and Access

The publication of this Article supposes the transfer of the copyright to ECORFAN-Mexico, SC in its Holding Taiwan for its ECORFAN Journal- Taiwan, which reserves the right to distribute on the Web the published version of the Article and the making available of the Article in This format supposes for its Authors the fulfilment of what is established in the Law of Science and Technology of the United Mexican States, regarding the obligation to allow access to the results of Scientific Research.

Article Title:

Name and Surnames of the Contact Author and the Co-authors	Signature
1.	
2.	
3.	
4.	

Principles of Ethics and Declaration of Solution to Editorial Conflicts

Editor Responsibilities

The Publisher undertakes to guarantee the confidentiality of the evaluation process, it may not disclose to the Arbitrators the identity of the Authors, nor may it reveal the identity of the Arbitrators at any time.

The Editor assumes the responsibility to properly inform the Author of the stage of the editorial process in which the text is sent, as well as the resolutions of Double-Blind Review. The Editor should evaluate manuscripts and their intellectual content without distinction of race, gender, sexual orientation, religious beliefs, ethnicity, nationality, or the political philosophy of the Authors.

The Editor and his editing team of ECORFAN® Holdings will not disclose any information about Articles submitted to anyone other than the corresponding Author.

The Editor should make fair and impartial decisions and ensure a fair Double-Blind Review.

Responsibilities of the Editorial Board

The description of the peer review processes is made known by the Editorial Board in order that the Authors know what the evaluation criteria are and will always be willing to justify any controversy in the evaluation process. In case of Plagiarism Detection to the Article the Committee notifies the Authors for Violation to the Right of Scientific, Technological and Innovation Authorization.

Responsibilities of the Arbitration Committee

The Arbitrators undertake to notify about any unethical conduct by the Authors and to indicate all the information that may be reason to reject the publication of the Articles. In addition, they must undertake to keep confidential information related to the Articles they evaluate.

Any manuscript received for your arbitration must be treated as confidential, should not be displayed or discussed with other experts, except with the permission of the Editor.

The Arbitrators must be conducted objectively, any personal criticism of the Author is inappropriate.

The Arbitrators must express their points of view with clarity and with valid arguments that contribute to the Scientific, Technological and Innovation of the Author.

The Arbitrators should not evaluate manuscripts in which they have conflicts of interest and have been notified to the Editor before submitting the Article for Double-Blind Review.

Responsibilities of the Authors

Authors must guarantee that their articles are the product of their original work and that the data has been obtained ethically.

Authors must ensure that they have not been previously published or that they are not considered in another serial publication.

Authors must strictly follow the rules for the publication of Defined Articles by the Editorial Board.

The authors have requested that the text in all its forms be an unethical editorial behavior and is unacceptable, consequently, any manuscript that incurs in plagiarism is eliminated and not considered for publication.

Authors should cite publications that have been influential in the nature of the Article submitted to arbitration.

Information services

Indexation - Bases and Repositories

RESEARCH GATE (Germany)
GOOGLE SCHOLAR (Citation indices-Google)
MENDELEY (Bibliographic References Manager)
HISPANA (Information and Bibliographic Orientation-Spain)

Publishing Services

Citation and Index Identification H
Management of Originality Format and Authorization
Testing Article with PLAGSCAN
Article Evaluation
Certificate of Double-Blind Review
Article Edition
Web layout
Indexing and Repository
ArticleTranslation
Article Publication
Certificate of Article
Service Billing

Editorial Policy and Management

69 Street. YongHe district, ZhongXin. Taipei-Taiwan. Phones: +52 1 55 6159 2296, +52 1 55 1260 0355, +52 1 55 6034 9181; Email: contact@ecorfan.org www.ecorfan.org

ECORFAN Journal-Taiwan

Reconstruction of motor voltage control signal in industrial applications using IoT
Camacho-Altamirano, Ulices, Martínez-Carrillo, Irma, Juárez-Toledo, Carlos and Hernández-Epigmenio, Miguel Ángel
Universidad Autónoma del Estado de México - Unidad Académica Profesional Tianguistenco

Thermoeconomic analysis in solar collector fields: a focus on constant flowrate and variable flowrate models
Lugo-Granados, Hebert Gerardo, Canizalez-Dávalos, Lázaro and Picón-Núñez, Martín
Autonomous University of Zacatecas
University of Guanajuato

Construction and development of an ultrasonic spray pyrolysis system for semiconductor thin films deposition to photovoltaic applications
Palacio-Sifuentes, David, Álvarez-Macias, Carlos, Rodríguez-Castro, Sergio and Martínez-López, Ricardo
Tecnológico Nacional de México/Instituto Tecnológico de La Laguna

Effect of the angle of solar irradiance on the photo generation of a photovoltaic module
Castillo-Campos, Nohemí Alejandra, Palacio-Sifuentes, David Isaac, Escobedo-Márquez, Diana Laura and Álvarez Macías, Carlos
Tecnológico Nacional de México/Instituto Tecnológico de La Laguna

2524-2121
ISSN 2524-2121

www.ecorfan.org